ARTICLES
https://doi.org/10.1038/s41589-020-00670-w
nature chemical biology

Check for updates

Cuticle thickness affects dynamics of volatile emission from petunia flowers

Pan Liao[1,7], Shaunak Ray[2,7], Benoît Boachon[1,6], Joseph H. Lynch[1,3], Arnav Deshpande[2], Scott McAdam[3,4], John A. Morgan[1,2] and Natalia Dudareva[1,3,5] ✉

The plant cuticle is the final barrier for volatile organic compounds (VOCs) to cross for release to the atmosphere, yet its role in the emission process is poorly understood. Here, using a combination of reverse-genetic and chemical approaches, we demonstrate that the cuticle imposes substantial resistance to VOC mass transfer, acting as a sink/concentrator for VOCs and hence protecting cells from the potentially toxic internal accumulation of these hydrophobic compounds. Reduction in cuticle thickness has differential effects on individual VOCs depending on their volatility, and leads to their internal cellular redistribution, a shift in mass transfer resistance sources and altered VOC synthesis. These results reveal that the cuticle is not simply a passive diffusion barrier for VOCs to cross, but plays the aforementioned complex roles in the emission process as an integral member of the overall VOC network.

Plants emit annually over 10^9 metric tons of volatile organic compounds (VOCs), thus substantially contributing to atmospheric chemistry and climate[1,2]. Released from flowers, fruits and vegetative tissues, VOCs play critical roles in plant fitness by attracting pollinators and other beneficial organisms, defending plants against herbivores and pathogens, facilitating plant–plant communication and protecting against abiotic stresses[3,4]. Due to the plethora of biological processes dependent on VOCs, chemical composition and quantity of emitted volatiles are species-, organ- and tissue-specific, developmentally and/or temporally regulated, and depend on biotic and abiotic factors[3,5–7]. Substantial progress has been made in understanding the biosynthesis of plant VOCs and their regulation[4,8], but much less is known about how volatiles are transported from cells into the atmosphere.

Although chemically diverse, VOCs are lipophilic low-molecular-weight (~100–200 Da) compounds with high vapor pressure at ambient temperature. To be released from cells, they must move from the site of synthesis through the cytosol, cross the plasma membrane, hydrophilic cell wall and finally the waxy cuticle[9]. Until recently, it was assumed that VOCs simply diffuse through each barrier. However, modeling of emission predicted that VOCs would accumulate to toxic levels in membranes in the absence of biological mediation due to their favorable partitioning into the lipid bilayers[9]. These in silico model predictions were experimentally validated in planta by downregulation of an ATP-binding cassette (ABC) transporter, PhABCG1, capable of transporting phenylpropanoid/benzenoid volatiles across the plasma membrane in petunia flowers[10].

The cuticle is the final physical barrier for VOCs to cross in most plant cells. Due to their hydrophobicity, the rate of VOC transport should depend on the physicochemical properties of the compound itself (diffusivity and solubility in the cuticle) and the cuticle composition and thickness[11–14]. Although cuticle structure and composition vary considerably between plants, organs and developmental stages, it is commonly composed of cutin and cuticular wax, the latter of which is embedded in and deposited on the surface of the cutin matrix[12,15]. The cuticular wax is a semicrystalline mixture of alkanes, aldehydes, primary and secondary alcohols, ketones and esters, all derived from very-long-chain fatty acids[14,16,17]. The cuticle generally acts as a molecular transport barrier, protecting tissues from stresses and preventing organ fusion during plant development[15]. While the role of the cuticle in transpirational water flux is well established[15,18] and extensive previous research provides knowledge about the interaction of atmospheric VOCs with the cuticle[19–23], how the cuticle is involved in the release of hydrophobic volatiles into the atmosphere remains an unresolved question.

Here, we use *Petunia hybrida* flowers, which emit high levels of phenylalanine- (Phe-) derived volatiles[24,25], to investigate the role of the cuticle in the emission process. We show that reduction in cuticle thickness not only alters VOC emission, but also leads to redistribution of VOC internal pools and feedback inhibition of VOC biosynthesis, demonstrating that the cuticle is an integral member of the overall emission network.

Results

Generation of petunia flowers with altered cuticles. Our mathematical modeling of VOC emission predicted that out of all barriers the cuticle imposes the highest resistance to VOC efflux[9], yet this has not been experimentally evaluated. To determine whether the cuticle of petunia flowers retains VOCs, their levels were analyzed in cuticular waxes of flowers on day 2 postanthesis, the developmental stage with the highest VOC emission[26]. This analysis revealed that the cuticle holds 53 ± 4% of total VOC internal pools (Fig. 1a).

Previous studies have shown that cuticle formation can be altered by perturbing transport of wax precursors from the site of their biosynthesis at the endoplasmic reticulum across the plasma membrane and through the cell wall to be deposited at the cell surface[27]. It is well established that transport of cuticular monomers across the plasma membrane requires ABC transporters[15].

[1]Department of Biochemistry, Purdue University, West Lafayette, IN, USA. [2]Davidson School of Chemical Engineering, Purdue University, West Lafayette, IN, USA. [3]Purdue Center for Plant Biology, Purdue University, West Lafayette, IN, USA. [4]Department of Botany and Plant Pathology, Purdue University, West Lafayette, IN, USA. [5]Department of Horticulture and Landscape Architecture, Purdue University, West Lafayette, IN, USA. [6]Present address: BVpam FRE 3727, Université de Lyon, Université Jean Monnet Saint-Etienne, CNRS, Saint-Etienne, France. [7]These authors contributed equally: Pan Liao, Shaunak Ray. ✉e-mail: dudareva@purdue.edu

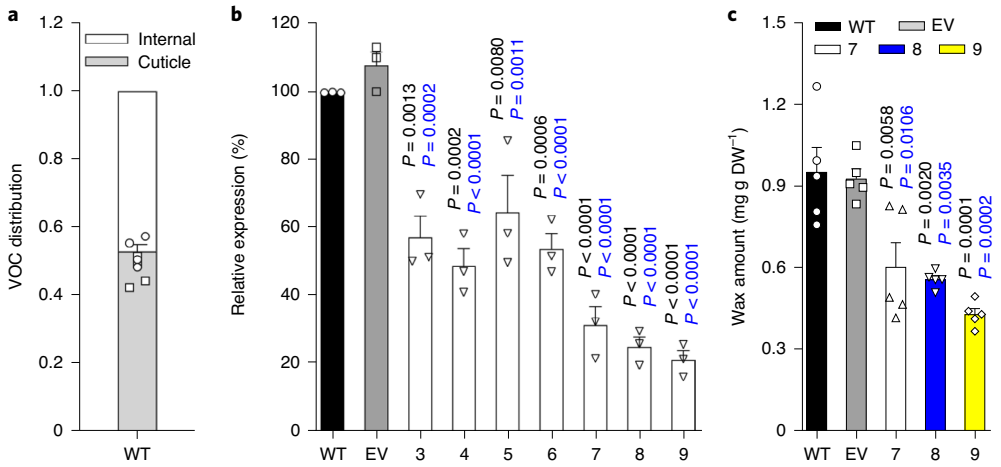

Fig. 1 | VOC distribution within cell and effect of *PhABCG12* downregulation on total wax amount in petunia flowers. a, Cellular VOC distribution in 2-day-old wild-type petunia flowers. Data are means ± s.e.m. ($n = 4$ biological replicates). **b**, *PhABCG12* messenger RNA levels determined by RT-qPCR in buds (3–4 cm) of wild-type (WT), EV control and seven independent *PhABCG12*-RNAi lines. Data are shown as a percentage of *PhABCG12* expression in WT set as 100% and are presented as means ± s.e.m. ($n = 3$ biological replicates). **c**, Total wax levels in 2-day-old flowers of WT, EV control and the three transgenic lines with greatest reduction in *PhABCG12* expression (lines 7, 8 and 9). Data are means ± s.e.m. ($n = 5$ biological replicates). *P* values were determined by two-way analysis of variance (ANOVA) with Tukey's multiple comparisons test relative to the WT (black) and EV (blue) controls.

In *Arabidopsis*, loss-of-function mutants of any of three closely related transporters, AtABCG11, AtABCG12 or AtABCG13, result in cuticle-deficient phenotypes[28–33]. Recently, we identified 17 ABCG transporters expressed in petunia flowers, two of which formed a clade with the three aforementioned *Arabidopsis* wax transporters[10]. These two putative petunia wax transporters, Ph9795 and Ph13519 are designated PhABCG11 and PhABCG12, respectively, as they exhibit 78/86% and 66/80% identity/similarity to AtABCG11 and AtABCG12, respectively. In addition, a blastn search against the genome of *P. axillaris*, the parent that mainly contributes to the *P. hybrida* genome[34], revealed three and one additional homologs of *AtABCG11* and *AtABCG12*, respectively. However, only *PhABCG11* and *PhABCG12* were expressed in *P. hybrida* corolla at high levels[35] (labeled as *PhABCG11a* and *PhABCG12b*, respectively, in Supplementary Tables 1 and 2). Expression of *PhABCG12* was 53% higher than *PhABCG11*, and both genes were developmentally regulated, with highest expression early in flower development, consistent with timing of cuticle formation (Supplementary Fig. 1a–c). Neither *PhABCG11* nor *PhABCG12* follow the developmental expression profile of scent biosynthetic genes, which have the highest levels on day 2 postanthesis[10,26]. Thus, *PhABCG11* and *PhABCG12* are promising targets for experimental perturbation of cuticle properties for subsequent analysis of the cuticle's role in VOC emission.

Our attempts to downregulate expression of each gene using the RNA interference (RNAi) approach under the control of a petal-specific promoter[36] resulted in no transgenic lines for *PhABCG11*, while seven lines were obtained for *PhABCG12*. Three lines, *PhABCG12-7*, *-8* and *-9*, with the greatest downregulation (68–79%) were selected for further analysis (Fig. 1b). *PhABCG12*-RNAi construct specifically targeted only *PhABCG12* (Supplementary Fig. 2a) without affecting *PhABCG12a* expression (Supplementary Fig. 2b). Unexpectedly, *PhABCG11* expression in *PhABCG12*-RNAi lines was coordinately decreased by 36–41% via an unknown mechanism (Supplementary Fig. 2c). Total wax loads in *PhABCG12*-RNAi lines were reduced by 35–55% relative to wild-type and empty vector (EV) control (Fig. 1c), while chemical composition and ratios between wax constituents were not significantly altered (Extended Data Fig. 1a,b). The flowers of transgenic plants displayed visible changes relative to wild-type and EV control. They were smaller, had less smooth surfaces, reduced fresh weight and more translucent petals (Fig. 2a upper panel and Extended Data Fig. 2a–d). Transmission electron microscopy (TEM) analysis of conical epidermal cells revealed a 22% reduction in cuticle thickness in petals of *PhABCG12-9*, the line with greatest *PhABCG12* downregulation, relative to wild-type (Fig. 2b,c and Extended Data Fig. 3). Toluidine blue staining, which detects increased cuticle permeability[37], showed that petals from transgenic lines, but not wild-type or EV control, exhibited Class II staining, characterized by a patchy and random pattern[37] (Fig. 2a lower panel). Cryogenic-scanning electron microscopy (cryo-SEM) of transgenic petals revealed that some epidermal cells lost their conical shape and became flattened (Supplementary Fig. 3). This morphological change was not uniform across the petal surface, but affected ~23% of the petal area (Supplementary Fig. 4), and may result from petal-to-petal fusion before flower opening, as was shown in cuticle-deficient mutants[30,32]. Consistent with reduced cuticle thickness, transgenic *PhABCG12*-RNAi flowers lost water faster than controls (Supplementary Fig. 5). However, phenotypic changes were not attributable to enhanced water loss, as transgenic plants grown in growth chamber with higher relative humidity did not recover the wild-type size phenotype, VOC emission and their internal pools (Supplementary Fig. 6). Since perturbing the cuticle could have pleiotropic effects on general cellular functions, we measured levels of total protein, sucrose, starch and chlorophyll, as well as petal respiration rate, seed yield and germination rate. All parameters remain unchanged in transgenic flowers relative to controls (Supplementary Fig. 7). Overall, these results demonstrate that altered cuticle thickness is the primary consequence of *PhABCG12*-RNAi downregulation, enabling analysis of the effect of cuticle on VOC emission.

Cuticle is an essential member of volatile network. Translocation of VOCs across the cuticle involves three physical processes: (1) partitioning of VOCs from the aqueous cell wall into the nonpolar waxes, (2) diffusion across the cuticle and (3) vaporization of the VOCs from the cuticle surface. It has been hypothesized that cuticular diffusion is the main barrier to VOC emission[9], and therefore a thinner cuticle was expected to permit increased VOC release. However, VOC profiling in *PhABCG12*-RNAi flowers revealed the opposite, total emission of VOCs was unexpectedly reduced

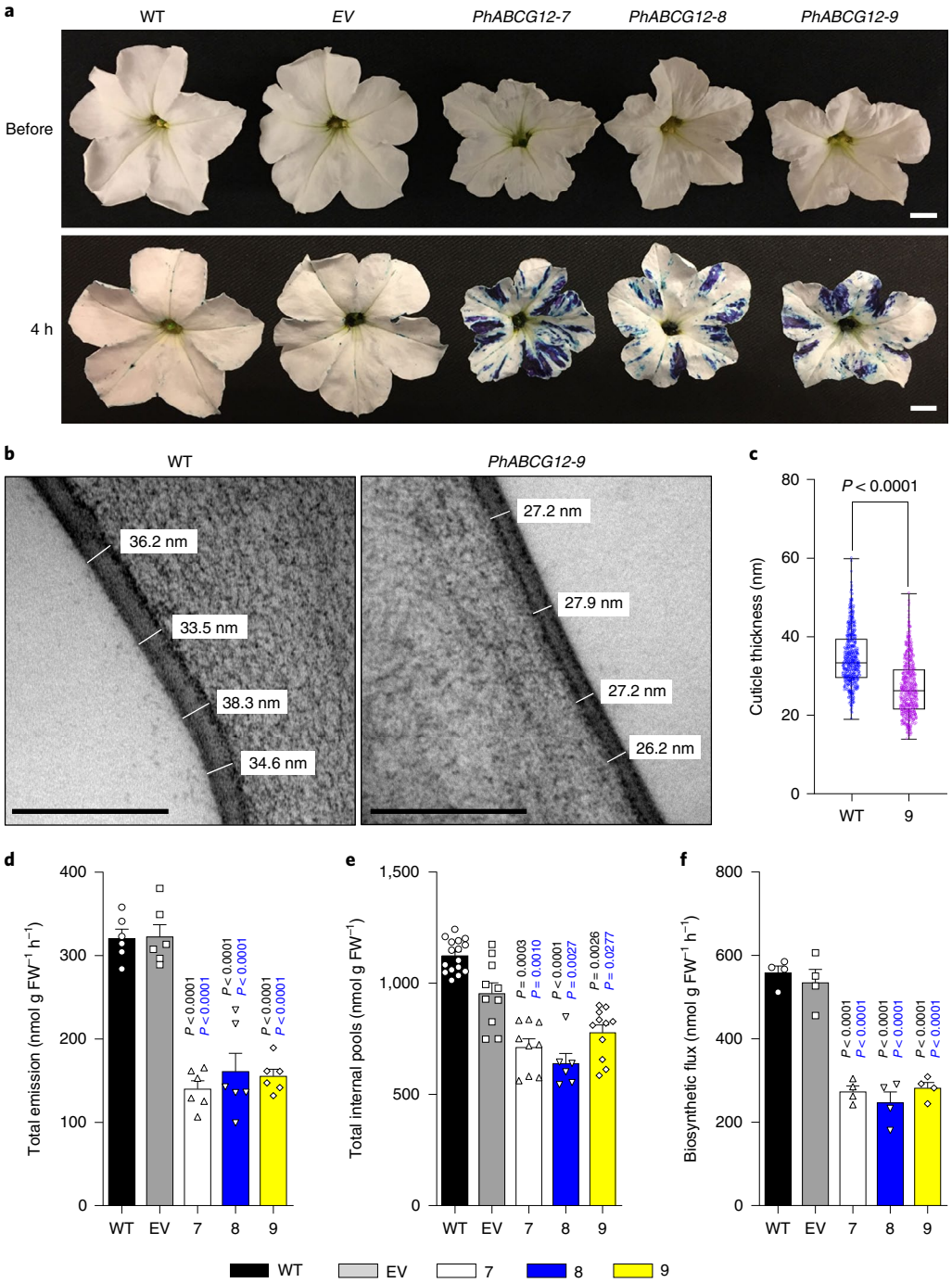

Fig. 2 | Effect of *PhABCG12* downregulation on flower phenotype, cuticle properties and scent network in petunia flowers. a, Representative 2-day-old petunia flowers from WT, EV control and three independent *PhABCG12*-RNAi lines (7, 8 and 9) before (upper panel) and 4 h after staining with toluidine blue (lower panel). Scale bar, 1 cm. **b**, Representative electron microscopy pictures of cross-sections of epidermal conical cells from adaxial petal surface of 2-day-old WT and *PhABCG12-9* flowers. Scale bar, 200 nm. **c**, Cuticle thickness measured in conical epidermal cells of 2-day-old WT and *PhABCG12-9* flowers as shown in **b**. The box represents the interquartile range of the data, whiskers show the minimum and maximum, and the line indicates the median ($n = 675$ measurements for each). *P* value was determined by unpaired two-tailed Student's *t*-test relative to control. **d**–**f**, Total emissions (**d**), total internal pools (**e**) and biosynthetic fluxes (**f**) in 2-day-old flowers from WT, EV control and three *PhABCG12*-RNAi lines 7, 8 and 9. Data are means ± s.e.m. ($n = 6$ biological replicates in **d**; in **e** $n = 16$, 10, 9, 6 and 11 biological replicates for WT, EV, lines 7, 8 and 9, respectively; and $n = 4$ biological replicates in **f**). *P* values in **d**, **e** and **f** were determined by two-way ANOVA with Tukey's multiple comparisons test relative to the WT (black) and EV (blue) controls.

by 50–56% (Fig. 2d) and their internal pools decreased by 31–43% relative to controls (Fig. 2e). Out of nine individual Phe-derived compounds emitted by petunia flowers, only two low-abundant compounds comprising <1% of total released VOCs, phenylethyl-benzoate and eugenol, remained unaffected by changes in cuticle thickness (Extended Data Fig. 4a,b). The effect of *PhABCG12*-RNAi downregulation on total VOC internal pools was opposite to that previously observed for RNAi downregulation of *PhABCG1*

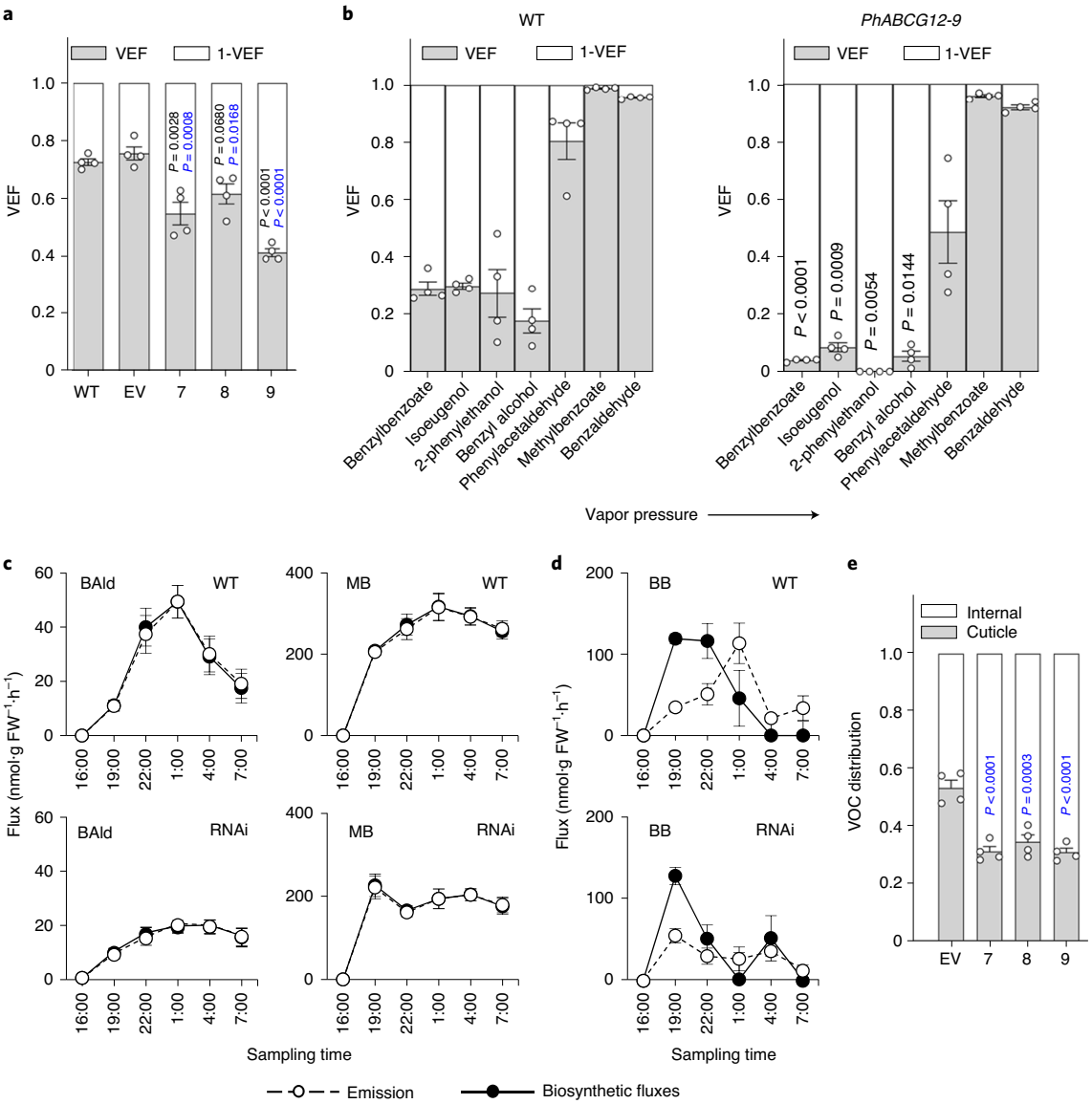

Fig. 3 | Effect of *PhABCG12* downregulation on VEFs, emission and biosynthetic fluxes of representative VOCs and cellular distribution of VOCs in 2-day-old petunia flowers. a, Overall VEF (the ratio of emission flux to the total biosynthetic flux) for WT, EV control and three independent *PhABCG12*-RNAi lines 7, 8 and 9. *P* values were determined by two-way ANOVA with the Tukey's multiple comparisons test relative to the corresponding WT (black) and EV (blue) controls. **b**, VEF of individual volatiles emitted by WT and *PhABCG12-9* flowers, shown in order of increasing compound volatility. *P* values were determined by unpaired two-tailed Student's *t*-test relative to the corresponding WT control. **c**,**d**, Emission and biosynthetic fluxes for benzaldehyde (BAld), methylbenzoate (MB) (**c**) and benzylbenzoate (BB) (**d**) in WT (upper panels) and *PhABCG12-9* line (lower panels). **e**, Cellular VOC distributions in petunia flowers of EV control and three independent *PhABCG12*-RNAi lines 7, 8 and 9. *P* values were determined by two-way ANOVA with the Tukey's multiple comparisons test relative to the corresponding EV control. All data are means ± s.e.m. ($n = 4$ biological replicates in **a**, **b** and **e** and $n = 3$ biological replicates in **c** and **d**).

transporter, which transports VOCs across plasma membrane[10], confirming differential effects of these two transporters on VOC emission.

Reduction in both emission and internal pools of VOCs in transgenics indicates that VOC formation is reduced. Indeed, evaluation of the total biosynthetic flux, determined as the sum of total emission and changes in corresponding internal pools over time, in control and transgenic flowers, showed that biosynthesis was reduced by 52 ± 7.8% in *PhABCG12*-RNAi flowers (Fig. 2f). To determine where in the scent biosynthetic network inhibition takes place, either upstream of volatile phenylpropanoid/benzenoid compound synthesis (Phe biosynthesis) or downstream of Phe (VOC biosynthesis), wild-type and *PhABCG12-9* flowers fed with $^{13}C_6$-Phe were subjected to metabolic flux analysis (Extended Data Fig. 5a,b). Similar total biosynthetic fluxes in wild-type and transgenic flowers after Phe feeding indicate that VOC biosynthetic capacity was not affected in *PhABCG12*-RNAi flowers (Extended Data Fig. 5c), suggesting that inhibition of VOC production occurred in the Phe biosynthetic network. This was verified by feeding 2-day-old wild-type and *PhABCG12-9* flowers with uniformly ^{13}C-labeled ([U-$^{13}C_6$]) glucose and analyzing Phe pool sizes and isotopic abundances. In both genotypes, the glucose labeling pattern was nearly identical (Supplementary Fig. 8a). Over the timecourse, there was little difference in Phe labeling, despite a 51% reduction in its pool size in transgenic petals at 22:00 (Supplementary Fig. 8b,c), indicating that indeed the carbon flux toward Phe is reduced in *PhABCG12-9*

petals. Quantitative PCR with reverse transcription (RT–qPCR) analysis of transcript levels of selected genes involved in Phe biosynthesis revealed that all of them were downregulated by 33 to 62% in *PhABCG12*-RNAi lines relative to control (Supplementary Fig. 9).

While $^{13}C_6$-Phe feeding compensated for reduced internal pools in transgenics and led to their similar isotopic labeling in control and transgenic petals, it did not restore emission in *PhABCG12*-RNAi flowers over 4 h despite its similar to control isotopic labeling (Extended Data Figs. 5d and 6a–d). If the cuticle is the primary resistance to net movement of volatiles out of the cell (mass transfer), it is expected that Phe feeding would result in higher VOC efflux from flowers with thinner cuticle. However, the lag in emission (Extended Data Fig. 6b), which resulted in the inability of transgenic flowers to catch up to wild-type levels of total emission despite rapid internal pool build up (Extended Data Fig. 6a), suggests the existence of transport limitation(s) upstream of cuticle. Indeed, expression of *PhABCG1*, encoding the plasma-membrane-localized VOC transporter, was reduced by 54% in transgenic flowers versus control (Supplementary Fig. 9), but total membrane transport capacity remains sufficient to sustain high emission under feeding conditions (Extended Data Fig. 6b).

Cuticle thickness affects dynamics of individual VOCs. To account for reduced VOC biosynthesis in comparative analysis of wild-type and transgenics, we defined a VOC emission factor (VEF) as the ratio of emission flux to corresponding total biosynthetic flux. A VEF value approaching one indicates that VOC emission is controlled mainly by biosynthesis, while VEF values lower than one reflect the existence of mass transfer limitations. Contrary to our hypothesis that a thinner cuticle would be more permeable to VOCs, *PhABCG12*-RNAi flowers displayed decreased VEF (Fig. 3a). Comparison of VEF of the individual volatiles in wild-type petals revealed that two compounds, methylbenzoate and benzaldehyde, have the highest values close to one (Fig. 3b). Out of all emitted compounds, they have the highest volatility based on vapor pressure (Supplementary Table 3) and were more abundant in the mixture of emitted volatiles with relatively small internal pools within the cell (Extended Data Fig. 4). Indeed, emission and biosynthetic fluxes overlaid for each of these two compounds when compared in wild-type petunia flowers (Fig. 3c), suggesting that methylbenzoate and benzaldehyde emissions are driven primarily by their biosynthesis with the cuticle providing limited resistance for release. In contrast, volatiles with lower ambient vapor pressures such as benzylbenzoate, isoeugenol, 2-phenylethanol and benzyl alcohol (Supplementary Table 3), had lower VEFs (Fig. 3b) and substantially larger internal pools relative to their corresponding emissions (Extended Data Fig. 4). Moreover, these compounds displayed a clear delay between the peak of biosynthesis and emission, and reduction in cuticle thickness did not change these patterns (Fig. 3d and Extended Data Fig. 7a,b), suggesting the existence of a mass transfer limitation for less volatile compounds. Thinner cuticles in transgenics had negligible effect on VEF of methylbenzoate and benzaldehyde, but decreased those of benzylbenzoate, isoeugenol, 2-phenylethanol and benzyl alcohol (Fig. 3b). Thus, the trend toward internal build up rather than emission for only compounds with lower volatility in transgenic petals (Fig. 3b) suggests that effect of cuticle thickness on VOC dynamics depends on physicochemical properties of compounds.

Analysis of VOC internal pools' distribution within the cell revealed that thinner cuticle holds a smaller proportion of VOCs, 32 ± 2% on average in transgenic plants (Fig. 3e) versus 53 ± 4% of total internal pools in wild-type flowers (Fig. 1a). Reduction in cuticle thickness decreased the relative cuticular abundance of all VOCs, although to different degrees, in transgenic petunia flowers relative to control (Extended Data Fig. 8a), leading to their accumulation within the cell. Previously, it was proposed and experimentally

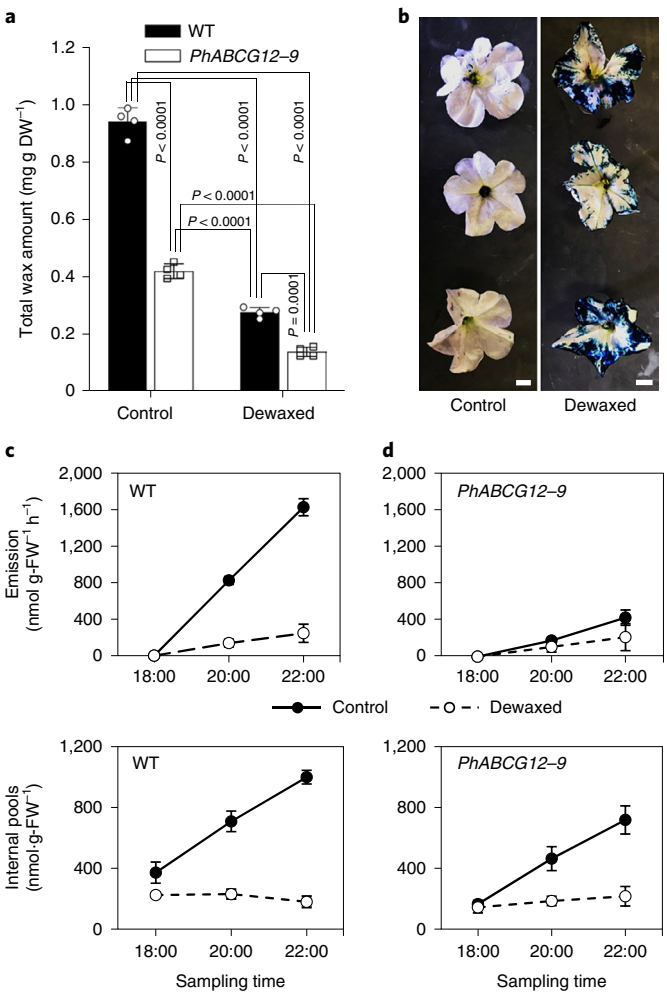

Fig. 4 | Effect of dewaxing on corolla wax levels, cuticle permeability, VOC internal pools and emissions in 2-day-old petunia flowers. a, Total wax levels before and after dewaxing of wild-type and *PhABCG12*-RNAi line 9 flowers. Data are means ± s.e.m. ($n = 4$ biological replicates). *P* values were determined by two-way ANOVA with Tukey's multiple comparisons test. **b**, Representative nondewaxed and dewaxed wild-type flowers 2 h after staining with toluidine blue. Scale bar, 1 cm. **c**,**d**, Emission fluxes and VOC internal pools over a 4-h period in nondewaxed and dewaxed wild-type (**c**) and *PhABCG12*-RNAi line 9 (**d**) flowers. Data are means ± s.e.m. ($n = 4$ biological replicates).

confirmed[9,10] that intracellular build up of VOCs has detrimental effects on membrane integrity. To test whether changes in VOC internal pools' distribution would lead to similar damaging effects despite an overall decrease in pool sizes in transgenic flowers, we performed staining with propidium iodide, which diffuses into cells and stains nucleic acids only if plasma membrane is disrupted[38]. Indeed, nuclei were stained in some cells of 2-day-old *PhABCG12-9* petunia petals but not in those of wild-type (Supplementary Fig. 10a). The similarity in round cell shape in transgenics and wild-type control, which does not have misshapen cells (Supplementary Fig. 3), suggests VOC toxicity occurs in the conical cells.

Internal pools of VOCs with relatively higher vapor pressures such as benzaldehyde and methylbenzoate were more abundant in the wild-type cuticle relative to the rest of the cell (>90% of total internal pools, despite their small overall internal pool sizes) when compared to that of less volatile compounds, and this trend was conserved in transgenic lines (Extended Data Fig. 8a). Cuticular VOC concentration is determined by the equilibria at both the

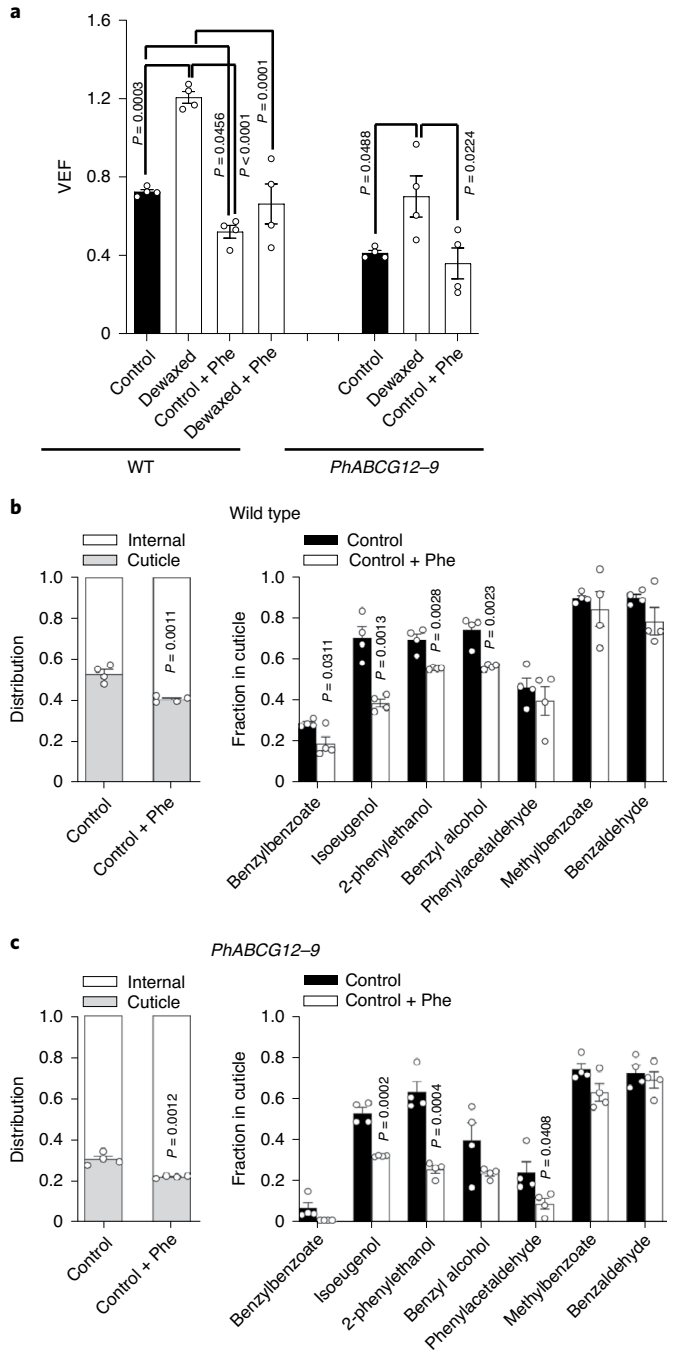

Fig. 5 | Effect of dewaxing and Phe feeding on VEFs and cellular VOC distributions in 2-day-old petunia flowers. a, Overall VEFs for control (nondewaxed) and dewaxed wild-type and *PhABCG12*-RNAi line 9 flowers with and without feeding with 150 mM Phe over a 4-h period from 18:00 until 22:00. Data are means ± s.e.m. ($n = 4$ biological replicates). *P* values were determined by two-way ANOVA with Tukey's multiple comparisons test. **b**,**c**, Cellular distributions of total (left panel) and individual VOCs (right panel) in control (nondewaxed) wild-type (**b**) and *PhABCG12-9* line (**c**) flowers with and without Phe feeding. Data are means ± s.e.m. ($n = 4$ biological replicates). *P* values were determined by unpaired two-tailed Student's *t*-test relative to the corresponding unfed control.

cuticle–atmosphere and cell wall–cuticle interfaces, which depend on compound relative volatility and octanol–water partition coefficient (as a proxy for wax–water partitioning), respectively. Comparisons of individual VOC distributions within the cell with corresponding compound volatility and octanol–water partition coefficient (Extended Data Fig. 8b,c) reveal that VOC volatility correlates with their partitioning in the cuticle. This suggests that the cuticle–atmosphere interface influences VOC distribution within the cell, consistent with the 'pulling' effect of the atmosphere on compounds with relatively high volatility.

Cuticle thickness affects rhythmicity of VOC emission. VOC emission from petunia flowers occurs in a rhythmic manner with highest flux at night[25,39]. To dissect the effect of reduced cuticle thickness on VOC dynamics around peak of emission, floral volatiles and their internal pools were analyzed in 2-day-old wild-type and *PhABCG12-9* flowers over a 15-h period. In wild-type flowers, a rapid accumulation of internal pools was observed between 16:00 and 22:00 and remained constant until 4:00 (Extended Data Fig. 9a). This increase in VOC internal pools correlated with a notable peak in emissions (Extended Data Fig. 9b) between 22:00 and 1:00, and such profile was conserved for all individual VOCs (Supplementary Fig. 11). In contrast, rhythmicity in VOC emission was practically absent in *PhABCG12*-9 flowers (Extended Data Fig. 9b), while internal pools exhibited a profile similar to wild-type, but with a roughly 27% lower maximum value (Extended Data Fig. 9a). Although transgenic petals still exhibited a clear temporal peak in VOC internal pools, the lack of a corresponding peak in emission suggests VOC redistribution upstream of the cuticle, thus dampening their release from the cell. Indeed, across six time points over a 15-h period, on average ~23% less VOCs were present in cuticle of *PhABCG12*-9 flowers than wild-type (Extended Data Fig. 9c), suggesting that limited cuticle sink for VOCs in transgenic flowers does not allow their rhythmic release.

Effect of solvent-based dewaxing on rate of VOC emission. In addition to the genetic approach, solvent-based dewaxing of petunia petals was used to examine the impact of reduced wax coverage on VOC emission without the potential influence of morphological changes observed in transgenic flower petals. These two approaches are complementary with their own strengths and limitations. Chemical dewaxing provides a snapshot of cuticle removal on VOC emission versus long-term changes in cuticle thickness in transgenics. Moreover, these two approaches have different starting points: in dewaxed flowers internal pools were instantaneously depleted, while in transgenic petals there is a constitutive shift in mass transfer resistance.

Dewaxing of wild-type petals removed 70 ± 6% of wax leading to susceptibility to toluidine blue staining (Fig. 4a,b) and a decrease in total VOC emission and internal pools by over 80% at the end of the 4-h collection period (Fig. 4c). To ensure that the decrease in VOC production is not due to a loss of petal metabolic potential during dewaxing process, the activity of phenylalanine ammonia lyase, which catalyzes the first committed step in the phenylpropanoid pathway, was measured before and 4 h after dewaxing and was found to be unchanged (Extended Data Fig. 10a). Moreover, feeding of dewaxed flowers with 150 mM Phe was able to recover both the VOC emission and biosynthetic fluxes observed in fed nondewaxed flowers (Extended Data Fig. 10b,c). The fact that Phe feeding of dewaxed flowers was able to recover only 62 ± 10% of VOC internal pools (Extended Data Fig. 10d), despite a similar to nondewaxed flowers absolute increase in internal pools on feeding (1,742 ± 52 nmol g fresh weight^{-1} [FW^{-1}] versus 1,510 ± 277 nmol g FW^{-1} in nondewaxed and dewaxed petals, respectively; Extended Data Fig. 10d,e), reflects the loss of the cuticular reservoir of VOCs. Taken together, these results demonstrate that (1) flowers remain metabolically active 4 h after dewaxing and (2) similar to *PhABCG12*-RNAi transgenic flowers removal of cuticle leads to decreased VOC production via

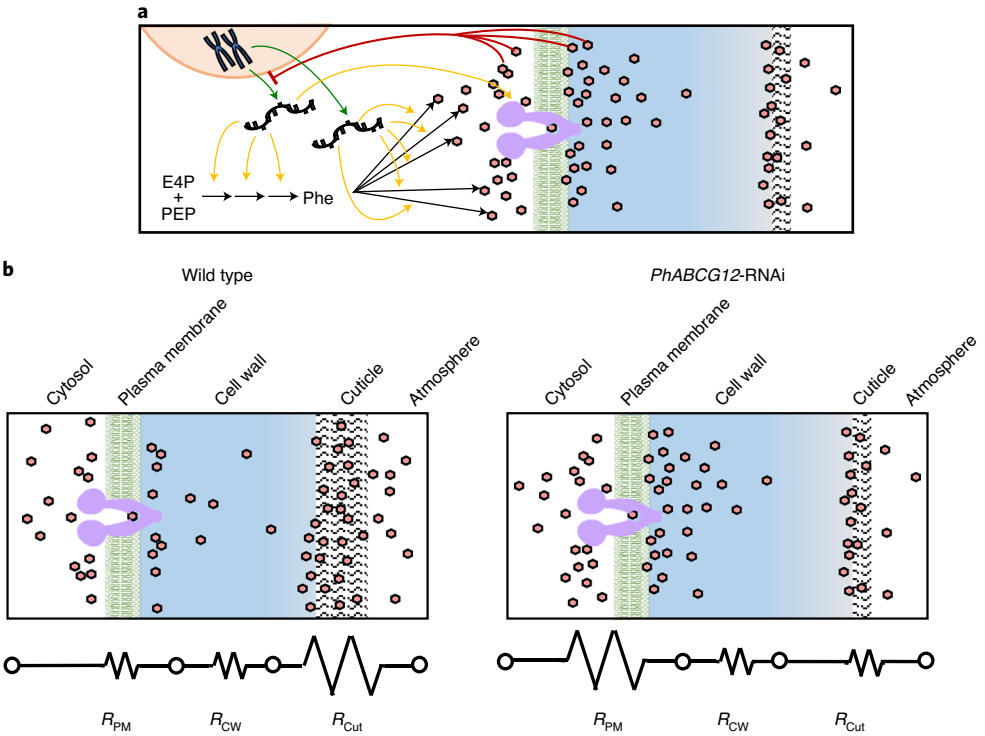

Fig. 6 | Schematic presentation of shift in the mass transfer resistance sources by reduction in cuticle thickness. a, Schematic representation of VOC (red icons) feedback effect on transcription of Phe biosynthetic genes. Black arrows represent enzymes, orange arrows represent RNA translation and green arrows represent gene transcription. Red lines show feedback inhibition of Phe biosynthetic gene transcription by accumulating VOCs via unknown mechanisms. **b**, Overall resistance shown by a resistance-in-series model. The barrier with the highest contribution to overall resistance to VOC (red icons) mass transfer out of the cells is shown by the largest resistor symbol. Purple icon in plasma membrane represents the previously characterized *PhABCG1* transporter[10].

feedback inhibition of Phe formation by internally accumulated volatile compounds. Indeed, carbon flux toward Phe was reduced after dewaxing. Although glucose was labeled 48% higher at 22:00 in dewaxed relative to nondewaxed wild-type petals, the ^{13}C labeling and pool sizes of Phe were both reduced by 84 and 38%, respectively, relative to the nondewaxed control (Supplementary Fig. 8). In addition, the expression of Phe biosynthetic genes, *ODO1* transcription factor and *PhABCG1* transporter was reduced by dewaxing (Supplementary Fig. 12) similar to the situation in *PhABCG12*-RNAi flowers (Supplementary Fig. 9). This effect could be replicated by inducing internal VOC accumulation to toxic levels via feeding of wild-type flowers with 15 mM benzaldehyde[10] (Supplementary Fig. 13). Moreover, as in *PhABCG12*-RNAi flowers, dewaxed petals display plasma-membrane disruption by internally accumulated VOCs, which is visible on propidium iodine staining (Supplementary Fig. 10b).

Reduced cuticle thickness shifts mass transfer resistance. Dewaxing of wild-type petunia petals led to an increase in VEF (Fig. 5a), as these flowers continue to emit VOCs, albeit at a low level, without changes in internal pools over the sampling time (Fig. 4c) further supporting the hypothesis that reduction of cuticle thickness decreases overall resistance. As petal dewaxing reduces VOC formation, to determine whether the high VEF value would be sustained under elevated VOC biosynthetic flux, dewaxed wild-type petunia petals were fed with 150 mM Phe. Unexpectedly, an increase in VOC biosynthesis decreased VEF (Fig. 5a), which could occur only if VOCs accumulate inside the cell in the absence of cuticle sink, thus demonstrating redistribution in the source of mass transfer resistance. VEF was also reduced in fed nondewaxed wild-type petunia petals relative to the nonfed control and was very similar to the VEF of dewaxed wild-type petals fed with Phe (Fig. 5a). Comparisons of individual VOC distributions within the cuticle with and without Phe feeding revealed that compounds with low relative volatility accumulate internally under high biosynthetic flux (Fig. 5b), suggesting a shift in mass transfer resistance source when VOC biosynthesis increased.

To test whether this effect was conserved in transgenic petals, *PhABCG12-9* RNAi flowers were subjected to dewaxing (Fig. 4a). Similar to wild-type flowers, dewaxing *PhABCG12-9* petals reduced emission and internal pool accumulation (Fig. 4d). Furthermore, dewaxing of transgenic petals increased VEF (Fig. 5a), but the value remained below one and was still lower than in control dewaxed petals. Thus, despite an 85% reduction in wax amount in *PhABCG12-9* petals by dewaxing relative to nondewaxed wild-type petals (Fig. 4a), VOCs still continue to accumulate internally (Fig. 4d). The inability to discharge the VOC internal pools after combined RNAi reduction of cuticle thickness and dewaxing suggests that the resistance to mass transfer in transgenic flowers has shifted from the cuticle to other sources, such as the plasma membrane and cell wall. Consistent with this conclusion, feeding of *PhABCG12-9* flowers with 150 mM Phe did not affect VEF (Fig. 5a) and, similar to wild-type petunia flowers, led to the redistribution of VOC internal pools of only compounds with low relative volatility (Fig. 5c).

Taken together, these results show that (1) cuticle serves as a important resistance barrier for VOC emission; (2) without enough cuticle present to act as a sink, VOCs accumulate internally, leading to inhibition of precursor formation to prevent toxicity; (3) compounds with lower relative volatility experience greater resistance at the cuticle and (4) other barriers, due to a shift in the mass transfer resistance, control emission under high VOC biosynthetic flux.

Discussion

The cuticle is the final barrier VOCs cross before being released into the atmosphere. Our results show that cuticle of petunia flowers holds >50% of internal VOCs (Fig. 1a), thus acting as the main site of VOC storage, and serving as a major source of mass transfer resistance. However, it mainly provides resistance to VOCs with low relative volatility with a negligible effect on highly volatile compounds, physiological emissions of which largely depend on their biosynthesis (Figs. 3 and 5 and Extended Data Fig. 8). The latter compounds have small internal pools relative to their emission flux, and these pools are predominantly allocated to the cuticle (Extended Data Fig. 8a). To sustain efficient emission, VOCs have to accumulate in the cuticle and decreasing the ability of cuticle to act as a concentrator/sink not only reduces overall emission (Figs. 2d and 4c), but also eliminates rhythmicity in VOC release (Extended Data Fig. 9b,c and Supplementary Fig. 11). The inability for VOCs, particularly those with low relative volatility, to build up in the cuticle due to a reduction in its thickness via RNAi downregulation of *PhABCG12* transporter (Fig. 2b,c) as well as dewaxing (Fig. 4a) leads to a redistribution of internal VOC pools (Figs. 3e and 5b and Extended Data Fig. 8a), thus resulting in cellular damage (Supplementary Fig. 10). To mitigate this detrimental effect, cells reduce production of VOCs by decreasing biosynthesis of the precursor Phe (Fig. 6a and Supplementary Figs. 8, 9 and 13), a feedback effect that was also observed in flowers after chemical dewaxing (Fig. 4 and Supplementary Figs. 8 and 12) but could be bypassed by Phe feeding (Extended Data Fig. 10b,d). Finally, the decrease in cuticle thickness leads to a shift in mass transfer resistance to other internal barriers (that is, plasma membrane and cell wall) (Fig. 6b), and this shift is more pronounced under high biosynthetic flux, likely reflecting the limited capacity of the plasma-membrane-localized VOC transporter, PhABCG1 (ref. [10]). Taken together, these results reveal that the cuticle, despite being a passive transport barrier, is nonetheless an integral member of the overall scent network.

Online content

Any methods, additional references, Nature Research reporting summaries, source data, extended data, supplementary information, acknowledgements, peer review information; details of author contributions and competing interests; and statements of data and code availability are available at https://doi.org/10.1038/s41589-020-00670-w.

Received: 5 March 2020; Accepted: 9 September 2020;
Published online: 19 October 2020

References

1. Zhao, D. F. et al. Environmental conditions regulate the impact of plants on cloud formation. *Nat. Commun.* **8**, 14067 (2017).
2. Guenther, A. B. et al. The model of emissions of gases and aerosols from nature version 2.1 (MEGAN2.1): an extended and updated framework for modeling biogenic emissions. *Geosci. Model Dev.* **5**, 1471–1492 (2012).
3. Dudareva, N., Negre, F., Nagegowda, D. A. & Orlova, I. Plant volatiles: recent advances and future perspectives. *Crc. Crit. Rev. Plant Sci.* **25**, 417–440 (2006).
4. Dudareva, N., Klempien, A., Muhlemann, J. K. & Kaplan, I. Biosynthesis, function and metabolic engineering of plant volatile organic compounds. *N. Phytol.* **198**, 16–32 (2013).
5. Staudt, M. & Bertin, N. Light and temperature dependence of the emission of cyclic and acyclic monoterpenes from holm oak (*Quercus ilex* L.) leaves. *Plant, Cell Environ.* **21**, 385–395 (1998).
6. Penuelas, J. & Llusia, J. Plant VOC emissions: making use of the unavoidable. *Trends Ecol. Evol.* **19**, 402–404 (2004).
7. Gouinguené, S. P. & Turlings, T. C. J. The effects of abiotic factors on induced volatile emissions in corn plants. *Plant Physiol.* **129**, 1296–1307 (2002).
8. Lynch J. H., Pichersky, E. & Dudareva, N. F. in *Biology of Plant Volatiles* (eds. Pichersky, E. & Dudareva, N.) 147–164 (CRC Press, 2020).
9. Widhalm, J. R., Jaini, R., Morgan, J. A. & Dudareva, N. Rethinking how volatiles are released from plant cells. *Trends Plant Sci.* **20**, 545–550 (2015).
10. Adebesin, F. et al. Emission of volatile organic compounds from petunia flowers is facilitated by an ABC transporter. *Science* **356**, 1386–1388 (2017).
11. Goodwin, S. M. et al. Cuticle characteristics and volatile emissions of petals in *Antirrhinum majus*. *Physiol. Plant.* **117**, 435–443 (2003).
12. Jeffree, C. E. in *Annual Plant Reviews* Vol. 23: *Biology of the Plant Cuticle* (eds. M. Riederer & C. Muller) 11–125 (Blackwell, 2006).
13. Martin, L. B. B. & Rose, J. K. C. There's more than one way to skin a fruit: formation and functions of fruit cuticles. *J. Exp. Bot.* **65**, 4639–4651 (2014).
14. Bernard, A. & Joubès, J. *Arabidopsis* cuticular waxes: advances in synthesis, export and regulation. *Prog. Lipid Res.* **52**, 110–129 (2013).
15. Yeats, T. H. & Rose, J. K. C. The formation and function of plant cuticles. *Plant Physiol.* **163**, 5–20 (2013).
16. Jenks, M. A., Eigenbrode, S. D. & Lemieux, B. Cuticular waxes of *Arabidopsis*. *Arabidopsis Book* **1**, e0016 (2002).
17. Li-Beisson, Y. et al. Acyl-lipid metabolism. *Arabidopsis Book* **11**, e0161 (2013).
18. Kerstiens, G. Water transport in plant cuticles: an update. *J. Exp. Bot.* **57**, 2493–2499 (2006).
19. Howells, D. J., Hambrook, J. L. & Allenby, E. A. Uptake of some volatile alkyl methylphosphonofluoridates from the vapour phase by wheat plants. *Pestic. Sci.* **7**, 349–354 (1976).
20. Sabljic, A., Guesten, H., Schoenherr, J. & Riederer, M. Modeling plant uptake of airborne organic chemicals. 1. Plant cuticle/water partitioning and molecular connectivity. *Environ. Sci. Technol.* **24**, 1321–1326 (1990).
21. Umlauf, G., Hauk, H. & Reissinger, M. The distribution of semivolatile organic compounds in conifer needles following gas phase contamination. *Chemosphere* **28**, 1689–1699 (1994).
22. Merk, S. & Riederer, M. Sorption of volatile C1 to C6 alkanols in plant cuticles. *J. Exp. Bot.* **48**, 1095–1104 (1997).
23. Platts, J. A. & Abraham, M. H. Partition of volatile organic compounds from air and from water into plant cuticular matrix: an LFER analysis. *Environ. Sci. Technol.* **34**, 318–323 (2000).
24. Boatright, J. et al. Understanding in vivo benzenoid metabolism in petunia petal tissue. *Plant Physiol.* **135**, 1993–2011 (2004).
25. Verdonk, J. C. et al. Regulation of floral scent production in petunia revealed by targeted metabolomics. *Phytochemistry* **62**, 997–1008 (2003).
26. Colquhoun, T. A. et al. Petunia floral volatile benzenoid/phenylpropanoid genes are regulated in a similar manner. *Phytochemistry* **71**, 158–167 (2010).
27. Javelle, M. et al. Overexpression of the epidermis-specific homeodomain-leucine zipper IV transcription factor OUTER CELL LAYER1 in maize identifies target genes involved in lipid metabolism and cuticle biosynthesis. *Plant Physiol.* **154**, 273–286 (2010).
28. Pighin, J. A. et al. Plant cuticular lipid export requires an ABC transporter. *Science* **306**, 702–704 (2004).
29. Bird, D. et al. Characterization of *Arabidopsis* ABCG11/WBC11, an ATP binding cassette (ABC) transporter that is required for cuticular lipid secretion. *Plant J.* **52**, 485–498 (2007).
30. Luo, B., Xue, X.-Y., Hu, W.-L., Wang, L.-J. & Chen, X.-Y. An ABC transporter gene of *Arabidopsis thaliana*, AtWBC11, is involved in cuticle development and prevention of organ fusion. *Plant Cell Physiol.* **48**, 1790–1802 (2007).
31. McFarlane, H. E., Shin, J. J. H., Bird, D. A. & Samuels, A. L. *Arabidopsis* ABCG transporters, which are required for export of diverse cuticular lipids, dimerize in different combinations. *Plant Cell* **22**, 3066–3075 (2010).
32. Panikashvili, D., Shi, J. X., Schreiber, L. & Aharoni, A. The *Arabidopsis* ABCG13 transporter is required for flower cuticle secretion and patterning of the petal epidermis. *N. Phytol.* **190**, 113–124 (2011).
33. Panikashvili, D. et al. The *Arabidopsis* DSO/ABCG11 transporter affects cutin metabolism in reproductive organs and suberin in roots. *Mol. Plant* **3**, 563–575 (2010).
34. Bombarely, A. et al. Insight into the evolution of the Solanaceae from the parental genomes of *Petunia hybrida*. *Nat. Plants* **2**, 16074 (2016).
35. Widhalm, J. R. et al. Identification of a plastidial phenylalanine exporter that influences flux distribution through the phenylalanine biosynthetic network. *Nat. Commun.* **6**, 8142 (2015).
36. Azuma, M. et al. A petal-specific InMYB1 promoter from Japanese morning glory: a useful tool for molecular breeding of floricultural crops. *Plant Biotechnol. J.* **14**, 354–363 (2016).
37. Tanaka, T., Tanaka, H., Machida, C., Watanabe, M. & Machida, Y. A new method for rapid visualization of defects in leaf cuticle reveals five intrinsic patterns of surface defects in *Arabidopsis*. *Plant J.* **37**, 139–146 (2004).
38. Rolny, N., Costa, L., Carrión, C. & Guiamet, J. J. Is the electrolyte leakage assay an unequivocal test of membrane deterioration during leaf senescence? *Plant Physiol. Biochem.* **49**, 1220–1227 (2011).
39. Kolosova, N., Gorenstein, N., Kish, C. M. & Dudareva, N. Regulation of circadian methyl benzoate emission in diurnally and nocturnally emitting plants. *Plant Cell* **13**, 2333–2347 (2001).

Methods

Plant materials and growth conditions. Wild-type and transgenic *P. hybrida* cv. Mitchell diploid (W115, Ball Seed Co.) were grown under standard greenhouse conditions with a light period from 6:00 to 21:00. Both *PhABCG11*-RNAi and *PhABCG12*-RNAi constructs were synthesized by Genscript. The *PhABCG11*-RNAi construct contained two spliced *PhABCG11* complementary DNA fragments corresponding to nucleotides 1,234–1,733 (in sense orientation) and 1,234–1,533 (in antisense orientation to form a hairpin structure), while *PhABCG12*-RNAi construct included two spliced *PhABCG12* cDNA fragments corresponding to nucleotides 225–724 (in sense orientation) and 225–524 (in antisense orientation), and both constructs were synthesized with flanking *AttL1* and *AttL2* sequences. Before synthesis, both the *PhABCG11* (PhABCG11a in Supplementary Table 1) and *PhABCG12* (PhABCG12b in Supplementary Table 1) constructs were verified to target only the desired genes and not to lead to off-target interference using the Sol Genomics Network VIGS Tool (http://vigs.solgenomics.net/). The analysis was performed by comparing the *PhABCG11a* and *PhABCG12b* RNAi target sequences against the *Petunia axillaris* and *P. inflata* (parents of *P. hybrida*) genomes[34] using default parameters, except that the n-mer setting was adjusted to 24 nucleotides, which is generally considered to be below the threshold to efficiently trigger downregulation[40,41]. This analysis revealed that no other genes would be targeted by the *PhABCG11* and *PhABCG12* double-stranded RNA triggers. In addition, the maximum stretch of uninterrupted shared sequence bewteen *PhABCG12* and *PhABCG11* as well as *PhABCG1* was found to be 12 nucleotides for each gene (Supplementary Fig. 2a). Further analysis of *PhABCG12b* RNAi downregulation on expression of *PhABCG12* homologs in *PhABCG12*-RNAi lines determined by RT–qPCR with gene-specific primers revealed that their expression remained unchanged (Supplementary Fig. 2b). Each of the synthetic RNAi fragments was placed under the control of the petal development-specific MYB1 promoter from Japanese morning glory (*Ipomoea nil*) (pDONRG-P4PIR-InMYB1pro vector, a kind gift from Y. Oshima)[36] in the binary destination vector R4pGWB5_stop_HSP[42] using the MultiSite Gateway Three-Fragment Vector Construction Kit (Invitrogen). Transgenic *P. hybrida* plants were obtained via *Argobacterium tumefaciens* (strain GV3101 carrying the final *PhABCG11*-RNAi or *PhABCG12*-RNAi constructs) leaf disc transformation using a standard transformation protocol[43].

Cuticular wax extraction and analysis. Waxes were extracted from petals of 2-day-old wild-type and transgenic petunia flowers at 18:00 by submerging corollas in 10 ml of high-performance liquid-chromatography- (HPLC-) grade hexane for 30 s. The solvent was decanted into a fresh glass vial and dried completely under a gentle stream of N_2. The dried wax residues were derivatized using 200 µl of *N,O*-bis(trimethylsilyl)trifluoroacetamide (BSTFA) (derivatization grade, Sigma-Aldrich) and pyridine (1:1 BSTFA:pyridine, v/v) for 15 min at 100 °C, and excess BSTFA and pyridine was evaporated under N_2. Derivatized waxes were solubilized in hexane containing a known quantity of the internal standard *n*-tetracosane (99%, Sigma-Aldrich) and samples were analyzed on an Agilent 6890 gas chromatograph (GC) equipped with a HP5-MS column (0.25 mm × 30 m × 0.25 µm, Agilent) and coupled to a 5975B inert MSD quadrupole mass spectrometer. The GC separation conditions were: an initial 2 min hold at 40 °C, followed by a 15 °C min^{-1} temperature ramp to 200 °C and held for 2 min, then increased at 3 °C min^{-1} to 320 °C, and held for 15 min. Compounds were identified based on retention times and fragmentation patterns, and quantified by peak areas relative to the internal standard. Specific correction (response) factors and calibration curves were developed from external standards of fatty acids, primary alcohols and *n*-alkanes of varying chain length and composition. Total wax quantity was obtained by pooling the wax extracts from 20 to 30 flowers in independent replicates, and measuring the weight of the dried residues.

RNA extraction and RT–qPCR analysis. Sample collection, RNA extraction and RT–qPCR was carried out as described previously[44] with minor modifications. Briefly, RNA was isolated from petals collected at the indicated developmental stages and times of the day using the Spectrum Plant Total RNA Kit (Sigma-Aldrich). Total RNA (2 µg) was treated by DNase I (Promega) before reverse transcription to cDNA using a 5× All-In-One RT MasterMix (Applied Biological Materials). Changes in *PhABCG11* and *PhABCG12* expression during flower development were analyzed by RT–qPCR using elongation factor 1-α (*EF1-α*) as a reference gene[45,46]. Relative quantification of *PhABCG1*, *PhABCG11*, *PhABCG12*, *PhDAHPS*, *PhEPSPS*, *PhCM1*, *PhCM2* and *PhODO1* transcripts were performed by RT–qPCR relative to the reference gene *PhUBQ10* (refs. [10,46]). RT–qPCR data were collected using StepOne v.2.2.2. and analyzed according to the $2^{-\Delta\Delta Ct}$ method[47]. The absolute quantification of gene transcript levels was performed based on standard curves generated by RT–qPCR with gene-specific primers using respective purified cDNA fragments diluted to several concentrations between 1.3 and 24.3 ng ml^{-1} for *PhABCG11* and 32.4 pg ml^{-1} to 608.0 ng ml^{-1} for *PhABCG12*. Absolute quantities of individual transcripts were calculated and expressed as pictograms (pg) of mRNA per 200 ng of total RNA. Primers used for RT–qPCR are listed in Supplementary Table 4.

TEM. Small pieces (1 mm in diameter) of wild-type and transgenic petals on day 2 postanthesis were fixed in 2% paraformaldehyde and 2% glutaraldehyde in 0.1 M sodium cacodylate buffer. After primary fixation, samples were rinsed and postfixed in buffered 1% osmium tetroxide containing 0.8% potassium ferricyanide. Subsequently, samples were dehydrated with a graded series of ethanol, transferred into acetonitrile and embedded in EMbed-812 resin. Thin sections (80 nm) were prepared on a Leica UC6 ultramicrotome and stained with 4% uranyl acetate and lead citrate. Sections were imaged on a FEI Tecnai T12 electron microscope equipped with a tungsten source and operating at 80 kV. Images were acquired in DM4 format on a Gatan Orius SC200 camera and converted to obtain TIFF files. To analyze cuticle thickness in conical epidermal cells from transgenic and wild-type petals, cuticle thickness shown in TEM images was measured by ImageJ software v.1.52a (ref. [48]).

Cryo-SEM. Wild-type and transgenic petals on day 2 postanthesis were mounted with OCT cryo-sectioning media on a flat specimen holder and cryo fixed by immersion in a nitrogen slush using a Gatan Alto 2500 Cryo-Preparation System (Gatan Inc.). Samples were immersed until liquid nitrogen boiling ceased, and then cryo transferred into the Gatan preparation chamber set at −170 °C. Samples were then immediately inserted into the SEM cryo stage set at −90 °C to sublimate surface frost and for initial viewing. Once frost free, samples were returned to the cryo-preparation chamber, allowed to cool and halt sublimation before sputter coating with a platinum target with 18 mA for 120 s at −170 °C. Final imaging was done at −140 °C with an accelerating voltage of 5 kV and spot size 3 on the Nova Nano 200 SEM.

Collection and analysis of plant volatiles. Floral volatile emission was analyzed by dynamic headspace collection of volatiles at 25 °C on columns containing 50 mg Poropak Q (80–100 mesh) (Sigma-Aldrich) and analyzed by GC–MS as described previously[10,49]. Briefly, emitted floral volatiles were collected from detached transgenic and control flowers on day 2 postanthesis from 18:00 to 22:00. Subsequently, ~280 µl dichloromethane containing 52 nmol of internal standard (naphthalene) was used to elute volatiles from collection columns for GC–MS analysis. Internal pools of volatiles from transgenic and control tissues collected at 22:00 h on day 2 postanthesis were extracted according to ref. [10] and quantified by GC–MS as described previously[49]. Briefly, 0.5 g of petal tissue was collected, ground to a fine powder in liquid nitrogen, and internal pools were extracted in 5 ml of dichloromethane containing 52 nmol of internal standard (naphthalene) for 12 h at 4 °C with shaking. Samples were concentrated to ~200 µl under a stream of nitrogen gas before analysis by GC–MS. All GC–MS data were collected and analyzed using Agilent MassHunter Workstation Software v.B.07.01.

Toluidine blue staining. Toluidine blue staining was performed following published protocol as follows[37,50]. Excised petals of petunia flowers on day 2 postanthesis collected at 15:00 were submerged in 0.05% toluidine blue aqueous solution. Flowers were incubated for 2 or 4 h, as indicated, before imaging.

Water loss measurement. Water loss measurements were carried out according to refs. [51,52] with some modifications. Two-day-old petunia flowers (three flowers per replicate) were detached and left in ambient laboratory conditions. The fresh weight of the flowers was recorded at the indicated times over 24 h to obtain total water loss rate.

Starch and sucrose quantification. Starch was extracted as described previously[53]. In brief, corolla tissue (collected on day 2 postanthesis at 15:00) was flash frozen in liquid nitrogen, ground to fine powder and 100 mg of powder was suspended in 1 ml 80% ethanol by vortexing. After heating at 100 °C for 3 min, samples were centrifuged at 4,000*g* for 15 min at room temperature, and the supernatant was discarded. This process was repeated five additional times. The final starch-containing pellet was resuspended in 1 ml water and the starch gelatinized by heating for 10 min at 100 °C. Starch was hydrolyzed by adding sodium acetate (pH 5.5) to a final concentration of 100 mM, along with 6 units of α-amyloglucosidase and 0.5 units of α-amylase, and incubated at 37 °C for 4 h. The hydrolyzed starch samples were centrifuged at 10,000*g* for 5 min at room temperature and a 20-µl sample was subjected to chromatographic separation using an Agilent 1260 Infinity II HPLC system and a Hi-Plex Ca column (300 × 7.7 mm; Agilent) held at 80 °C with water as the isocratic mobile phase. Glucose was detected using an Agilent 1260 Refractive Index Detector.

Sucrose was extracted and analyzed as described previously[54]. In brief, corolla tissue (collected on day 2 postanthesis at 15:00) was flash frozen in liquid nitrogen and ground to fine powder. Then 0.5 ml of methanol containing 1 mg ml^{-1} of sorbitol as internal standard was used to extract 100 mg of the homogenized tissue at 70 °C for 15 min. After cooling, 0.5 ml of water was added and the sample was incubated at room temperature for an additional 15 min with periodic vortexing. Samples were centrifuged at 12,000*g* for 15 min at room temperature, and 20 µl of the supernatant was dried under a gentle flow of nitrogen. The resulting residue was derivatized by adding 50 µl of pyridine containing 20 mg ml^{-1} methoxyamine hydrochloride and incubating for 30 min at 30 °C, followed by additional 90 min incubation at 37 °C in the presence of 50 µl of *N*-trimethylsilyl-*N*-methyl trifluoroacetamide. Derivatized samples were analyzed by GC–MS by introducing 1 µl of sample into the GC injector held at 230 °C in split mode using a split ratio

of 1:4. The column temperature was held at 150 °C for 1 min and then increased at 5 °C min^{-1} to 175 °C, 1 °C min^{-1} to 185 °C and 10 °C min^{-1} to 250 °C.

Respiration rate measurements. Petal respiration rates were measured using an infrared gas analyzer (LI-6800, Licor). Petals of flowers on plants grown in greenhouse conditions were enclosed in the cuvette and CO_2 efflux was measured after stability of environmental parameters in the cuvette. Conditions in the cuvette were maintained as close to greenhouse environmental conditions as possible, a light intensity was set a 1,000 µmol quanta m^{-2} s^{-1}, temperature was maintained at 25 °C and vapor pressure difference controlled at 1.2 kPa. Respiration rates were measured for each petal after gas exchange parameters stabilized, which occurred within approximately 5 min after enclosure of petal inside the cuvette. All data were standardized against petal area in the cuvette.

Seed germination assays. Seeds of petunia wild-type and three independent *PhABCG12*-RNAi lines (7, 8 and 9) (210 seeds per line) were sterilized in 75% ethanol, rinsed in sterile water five times and placed on plates containing MS agar with 3% sucrose (42 seeds per plate). After cold stratification at 4 °C for 5 d, seed were transferred to a growth room (21 °C, 8-h dark/22 °C 16-h light). The radicle emergence was considered as germination. The number of germinated seeds was recorded every 24 h within 7 d.

Analysis of seed yield. Seed yield was measured as described previously[55] with minor modifications. Briefly, flowers were cross-pollinated at 18:00 on day 2 postanthesis. After 4–5 weeks, mature seed pods with brown color were collected individually and placed in a Office Depot Brand Coin Envelope (5.7 × 8.9 cm^2). Seeds were collected and dried for 2 d at 37 °C after pods were cracked. Subsequently, the weight of total seeds per pod, seed weight and total number of seeds per pod were measured.

Analysis of chlorophyll levels. Chlorophyll levels were measured according to ref. [56] with minor modifications. Briefly, wild-type and transgenic petals collected at 15:00 on day 2 postanthesis were ground to fine powder in liquid nitrogen and chlorophylls were extracted in dim light by adding two lots of 500 µl of 80% aqueous acetone to 100 mg of sample powder. After centrifugation at 12,000*g* for 10 min, supernatants were combined and the concentration of chlorophyll a and b were determined by spectrophotometrically at 663 and 645 nm, respectively, using a Nanodrop 2000c spectrophotometer (Thermo Scientific). The total chlorophyll levels were calculated according to ref. [56].

Propidium iodide staining and confocal laser scanning microscopy. Petals of wild-type and *PhABCG12*-RNAi flowers collected at 15:00 on day 2 postanthesis were stained in propidium iodide solution (10 µg ml^{-1}, Invitrogen) for 1 h with shaking at room temperature. Confocal fluorescence microscopy was performed as described previously[10,57] with minor modifications. Briefly, propidium iodide-stained samples were excited with a 561-nm laser and images were recorded by a 617/73 emission filter using a Zeiss LSM 880 Upright Confocal system and operated using Zeiss Efficient Navigation (ZEN)-Black Edition software (Zen 2.3 SP1, Carl Zeiss Inc.).

Dewaxing of petunia petals. To determine the quantity of volatiles in petunia epicuticular waxes, petals on day 2 postanthesis were rapidly dipped in hexane (<5 s) and then were lightly dried under the fume hood to remove excess hexane. Care was taken to prevent full submersion of petals so that only the adaxial surface of the flower touched the solvent. Hexane pools were independently profiled for volatiles and wax quantity using GC–MS as described above, while dewaxed petals were sampled for VOC internal pools and emissions as described above. Total cuticular volatile fractions were determined according to the formula:

$$\text{Cuticular VOC fraction} = \frac{C_i^{\text{hex}}}{C_i^{\text{total}}} \times \frac{1}{R} \quad (1)$$

where C_i^{hex} is the volatile pool in the hexane fraction, C_i^{total} is the total volatile pool and R is the fraction of the total wax recovered during the dewaxing.

To test whether dewaxed flowers retained biosynthetic capability, dewaxed wild-type petals were fed with 15 and 150 mM Phe and VOC internal pools and emission were subsequently analyzed between 18:00 and 22:00. In addition, PAL activity was measured in dewaxed and nondewaxed wild-type petals on day 2 postanthesis as described previously[39,54], except that assays were adapted to HPLC detection of cinnamic acid formation from L-Phe. In brief, 100 µl of reaction mixture containing protein samples from dewaxed and nondewaxed petals (5–30 µg), 2 mM L-Phe and 0.1 M sodium borate (pH 8.8) was incubated at room temperature for 1 h and then terminated by adding 5 µl of 6 M HCl. After centrifugation, 10 µl of the supernatant was analyzed by HPLC equipped with the Agilent Poroshell 120 EC-C18 column (3.0 mm × 150 mm × 2.7 µm) held at 35 °C using an 8-min linear gradient of 5–70% acetonitrile in 0.1% formic acid at a flow rate of 0.4 ml min^{-1}. Cinnamic acid was detected by ultraviolet absorbance at 270 nm and quantified using Open LAB CDS Chemstation Rev. C.01.08(210) and authentic standard. Control assays including (1) with all reaction components with boiled protein extracts; (2) with all reaction components except protein extracts and (3) with all components except for L-Phe, did not produce cinnamic acid.

Metabolic flux analysis with $^{13}C_6$-phenylalanine labeling. Wild-type and *PhABCG12*-RNAi-9 petunia corollas excised from flowers 2 d postanthesis were placed in a cut 1.7-ml Eppendorf tube containing 300 µl of a solution of 150 mM ring-labeled $^{13}C_6$-Phe (Cambridge Isotope Laboratories). Emitted and internal pools of volatiles were collected between 18:00 and 22:00 as described above at 60-, 120- and 240-min time points after start of feeding and analyzed by GC–MS. Labeled volatiles were identified by M+6 and M+12 (for VOCs with two aromatic rings) shifts in m/z and labeling percentage was determined based on the peak areas of labeled and unlabeled volatiles. Metabolic fluxes were calculated by applying mass balances and in vivo metabolite labeling profiles as described previously[24]. Emission fluxes and time-dependent accumulation of internal pools were estimated using linear regression, with the variances of the estimated slopes calculated using the standard linear regression procedure described previously[58]. As fluxes are a function of the linear regression and other experimental measurements, flux variances are derived by considering the propagation of errors based on equation (2):

$$\sigma_y^2 = \sum_{i=1}^{n} \sigma_{x_i}^2 \left(\frac{\partial y}{\partial x_i}\right)^2 \quad (2)$$

where $y = f(x_1,\ldots,x_n)$.

Benzaldehyde feeding. Wild-type petunia corollas on day 2 postanthesis were collected at 9:00 and fed with 0 and 15 mM of benzaldehyde for 6 h, as described previously[10]. Mock and benzaldehyde-fed petunia corollas were collected at 15:00, ground to a fine powder in liquid nitrogen and used for subsequent RNA extraction, cDNA synthesis and RT–qPCR analysis as described above.

Stable isotope labeling with ^{13}C-glucose. Corollas from flowers 2 d postanthesis were placed, cut surface down, on filter paper moistened with 3% (w/v) uniformly labeled $^{13}C_6$-glucose (Cambridge Isotope Laboratories, Inc.) at 18:00. After 1, 2 and 4 h, glucose was extracted and analyzed as described for sucrose above. Phe was extracted and analyzed as described previously[59] with some modifications as follows. Tissue was extracted with 10 µl mg^{-1} of 75% methanol (v/v) containing 1 µg ml^{-1} of *p*-fluoro-DL-phenylalanine as internal standard. After a 30-min incubation at 65 °C, samples were centrifuged at 15,000*g* for 15 min. The supernatant was transferred to a separate tube, dried to completeness in a Labconco CentriVap concentrator, resuspended in ultrapure water with 20% (v/v) methanol and 10 µl of sample was injected into LC–MS/MS. The incorporation of the ^{13}C-labeled glucose in the shikimate pathway was estimated by determining the percentage ^{13}C label in phenylalanine via reverse-phase chromatography on a Shimadzu HPLC-20 AD (Shimadzu) coupled to a AB Sciex 5500 mass spectrometer (AB Sciex) with electrospray ionization in negative ion mode. The ionization parameters were manually tuned and are listed in the Supplementary Table 5. Chromatographic separations were performed on a 150 mm × 4.6 mm Zorbax Eclipse C_8 column, with 5 µm particles (Agilent Technologies), at a column temperature 30 °C and a flow rate of 1 ml min^{-1}. A linear gradient of aqueous solvent A (2.5 mM ammonium acetate in ultrapure water, adjusted to pH 5.3 with acetic acid) and organic solvent B (97.8% acetonitrile, 2% ultrapure water and 0.2% formic acid) was as follows: 10% B (v/v) for 1 min, 10–20% B over 6 min, 20–20.8% B over 9 min, 20.8–50% B over 1 min, 50–70% B over 1 min, hold at 70% B for 3 min, return to 10% B over 2 min followed by equilibration at 10% B for 3 min for a total of 26 min. The peaks were integrated and quantified by Analyst v.1.5.1 software. For quantifying %C labeling, all the possible Q1/Q3 combinations were considered. Labeling of both glucose and Phe were corrected for natural isotope abundance.

Calculation of volatile emission factor. Biosynthetic and emission fluxes were estimated from dynamic sampling of volatile internal pools and emissions from detached transgenic and control petunia flowers on day 2 postanthesis from 18:00 to 22:00. Time-dependent accumulation of volatile internal pools and the rate of emission were estimated using linear regression, with propagation of regression and experimental errors calculated using equation (2). Biosynthetic flux was determined from the mass balance for an individual volatile:

$$\frac{dC_i}{dt} = \nu_{\text{syn},i} - \nu_{\text{emi},i} \quad (3)$$

where $\nu_{\text{syn},i}$ and $\nu_{\text{emi},i}$ are the biosynthetic and emission fluxes of a volatile compound i, respectively. Emission and biosynthetic fluxes for individual compounds are shown in Supplementary Fig. 14. The VEF is the ratio between the emission and biosynthesis of a volatile compound:

$$\text{VEF}_i = \frac{\nu_{\text{emi},i}}{\nu_{\text{syn},i}} \quad (4)$$

The overall VEF is determined as the ratio between the sum of all individual volatile emission fluxes and the sum of all individual volatile biosynthetic fluxes:

$$\mathrm{VEF} = \frac{\sum_{i=1}^{n} v_{\mathrm{emi},i}}{\sum_{i=1}^{n} v_{\mathrm{syn},i}} \quad (5)$$

where n denotes the number of volatiles detected in the pools and headspace of petunia flowers.

Measurement of flower fresh weight, corolla diameter and corolla fresh weight. Flower fresh weight and corolla diameter of wild-type, EV control and three independent *PhABCG12*-RNAi lines (7, 8 and 9) were measured on 2-day-old detached flowers collected at 18:00. Corolla fresh weight of all the above lines was recorded at 22:00 for 2-day-old detached flowers after scent collection.

High humidity experiment. To test whether the phenotypic changes in *PhABCG12*-RNAi lines were caused by water stress, 2-month-old wild-type and three independent *PhABCG12*-RNAi lines (7, 8 and 9) were moved from standard greenhouse conditions with a normal humidity (<50%) to a growth chamber with a high relative humidity (75%) and allowed to acclimate for 1 week. Then, 2-day-old flowers were collected at 18:00 and flower fresh weight was recorded as well as total VOC emission, and internal pools were analyzed as described before and compared to that of control 2-day-old flowers growing in the standard greenhouse conditions with normal humidity.

Reporting Summary. Further information on research design is available in the Nature Research Reporting Summary linked to this article.

Data availability

We declare that all the data supporting the funding of this study are available within the paper and its supplementary information files or from the corresponding author upon reasonable request. *P. axillaris* genomic data were obtained from http://solgenomics.net using the *P. axillaris* v.1.6.2 genome database. Source data are provided with this paper.

References

40. Parrish, S., Fleenor, J., Xu, S., Mello, C. & Fire, A. Functional anatomy of a dsRNA trigger. *Mol. Cell* **6**, 1077–1087 (2000).
41. Segal, G., Song, R. & Messing, J. A new opaque variant of maize by a single dominant RNA-interference-inducing transgene. *Genetics* **165**, 387–397 (2003).
42. Oshima, Y. et al. Novel vector systems to accelerate functional analysis of transcription factors using chimeric repressor gene-silencing technology (CRES-T). *Plant Biotechnol.* **28**, 201–210 (2011).
43. Horsch, R. B. et al. A simple and general method for transferring genes into plants. *Science* **227**, 1229–1231 (1985).
44. Klempien, A. et al. Contribution of CoA ligases to benzenoid biosynthesis in petunia flowers. *Plant Cell* **24**, 2015–2030 (2012).
45. Qualley, A. V., Widhalm, J. R., Adebesin, F., Kish, C. M. & Dudareva, N. Completion of the core ß-oxidative pathway of benzoic acid biosynthesis in plants. *Proc. Natl Acad. Sci. USA* **109**, 16383–16388 (2012).
46. Qian, Y. et al. Completion of the cytosolic post-chorismate phenylalanine biosynthetic pathway in plants. *Nat. Commun.* **10**, 15 (2019).
47. Schmittgen, T. D. & Livak, K. J. Analyzing real-time PCR data by the comparative CT method. *Nat. Protoc.* **3**, 1101–1108 (2008).
48. Abràmoff, M. D., Magalhães, P. J. & Ram, S. J. Image processing with ImageJ. *Biophotonics Int.* **11**, 36–42 (2004).
49. Orlova, I. et al. Reduction of benzenoid synthesis in petunia flowers reveals multiple pathways to benzoic acid and enhancement in auxin transport. *Plant Cell* **18**, 3458–3475 (2006).
50. Li-Beisson, Y. et al. Nanoridges that characterize the surface morphology of flowers require the synthesis of cutin polyester. *Proc. Natl Acad. Sci. USA* **106**, 22008–22013 (2009).
51. Wang, Z.-Y., Xiong, L., Li, W., Zhu, J.-K. & Zhu, J. The plant cuticle is required for osmotic stress regulation of abscisic acid biosynthesis and osmotic stress tolerance in *Arabidopsis*. *Plant Cell* **23**, 1971–1984 (2011).
52. Zhang, J.-Y. et al. Overexpression of WXP1, a putative *Medicago truncatula* AP2 domain-containing transcription factor gene, increases cuticular wax accumulation and enhances drought tolerance in transgenic alfalfa (*Medicago sativa*). *Plant J.* **42**, 689–707 (2005).
53. Lynch, J. H. et al. Modulation of auxin formation by the cytosolic phenylalanine biosynthetic pathway. *Nat. Chem. Biol.* **16**, 850–856 (2020).
54. Maeda, H. et al. RNAi suppression of arogenate dehydratase1 reveals that phenylalanine is synthesized predominantly via the arogenate pathway in petunia petals. *Plant Cell* **22**, 832–849 (2010).
55. Boachon, B. et al. Natural fumigation as a mechanism for volatile transport between flower organs. *Nat. Chem. Biol.* **15**, 583–588 (2019).
56. Arnon, D. I. Copper enzymes in isolated chloroplasts. Polyphenoloxidase in *Beta vulgaris*. *Plant Physiol.* **24**, 1–15 (1949).
57. Yanagisawa, M. et al. Patterning mechanisms of cytoskeletal and cell wall systems during leaf trichome morphogenesis. *Nat. Plants* **1**, 15014 (2015).
58. Press, W. H. *Numerical Recipes: The Art of Scientific Computing* (Cambridge Univ. Press, 2007).
59. Jaini, R., Wang, P., Dudareva, N., Chapple, C. & Morgan, J. A. Targeted metabolomics of the phenylpropanoid pathway in *Arabidopsis thaliana* using reversed phase liquid chromatography coupled with tandem mass spectrometry. *Phytochem. Anal.* **28**, 267–276 (2017).

Acknowledgements

This work was supported by grant from the National Science Foundation no. IOS-1655438 to N.D. and J.A.M. and by the USDA National Institute of Food and Agriculture Hatch Project no. 177845 to N.D. We acknowledge the use of the imaging facilities of the Bindley Bioscience Center, a core facility of the NIH-funded Indiana Clinical and Translational Sciences Institute, for collection of confocal microscopy images. We thank Y. Oshima (National Institute of Advanced Industrial Science and Technology, Japan) for providing pDONOR_P4PIR-InMYB1pro and R4pGWB5_stop_HSP vectors. We thank R. Seiler and L. Mueller for technical assistance on SEM and TEM, respectively.

Author contributions

B.B., J.A.M. and N.D. conceived the project and designed research. P.L. performed analysis of flower phenotypes, protein levels, seed production and germination rates, VOC emission and their internal pools, internal cellular VOC distribution over a 15 h period, toluidine and propidium iodide staining experiments, expression analysis and feeding experiments. S.R. performed wax profiling, VOC distribution and metabolic flux analyses, dewaxed experiments, water loss determination and analyzed rhythmicity of VOC production and accumulation. B.B. generated *PhABCG12*-RNAi lines and performed initial expression and metabolic profiling. J.H.L. performed analysis of sucrose and starch levels as well as flux through the shikimate pathway. A.D. run and analyzed samples for shikimate pathway flux experiments. S.M. analyzed respiration rate. P.L., S.R, B.B., J.H.L., A.D., S.M., J.A.M. and N.D. analyzed data. N.D. wrote the manuscript with contribution from all authors. All authors read and edited the manuscript.

Competing interests

The authors declare no competing interests.

Additional information

Extended data is available for this paper at https://doi.org/10.1038/s41589-020-00670-w.

Supplementary information is available for this paper at https://doi.org/10.1038/s41589-020-00670-w.

Correspondence and requests for materials should be addressed to N.D.

Reprints and permissions information is available at www.nature.com/reprints.

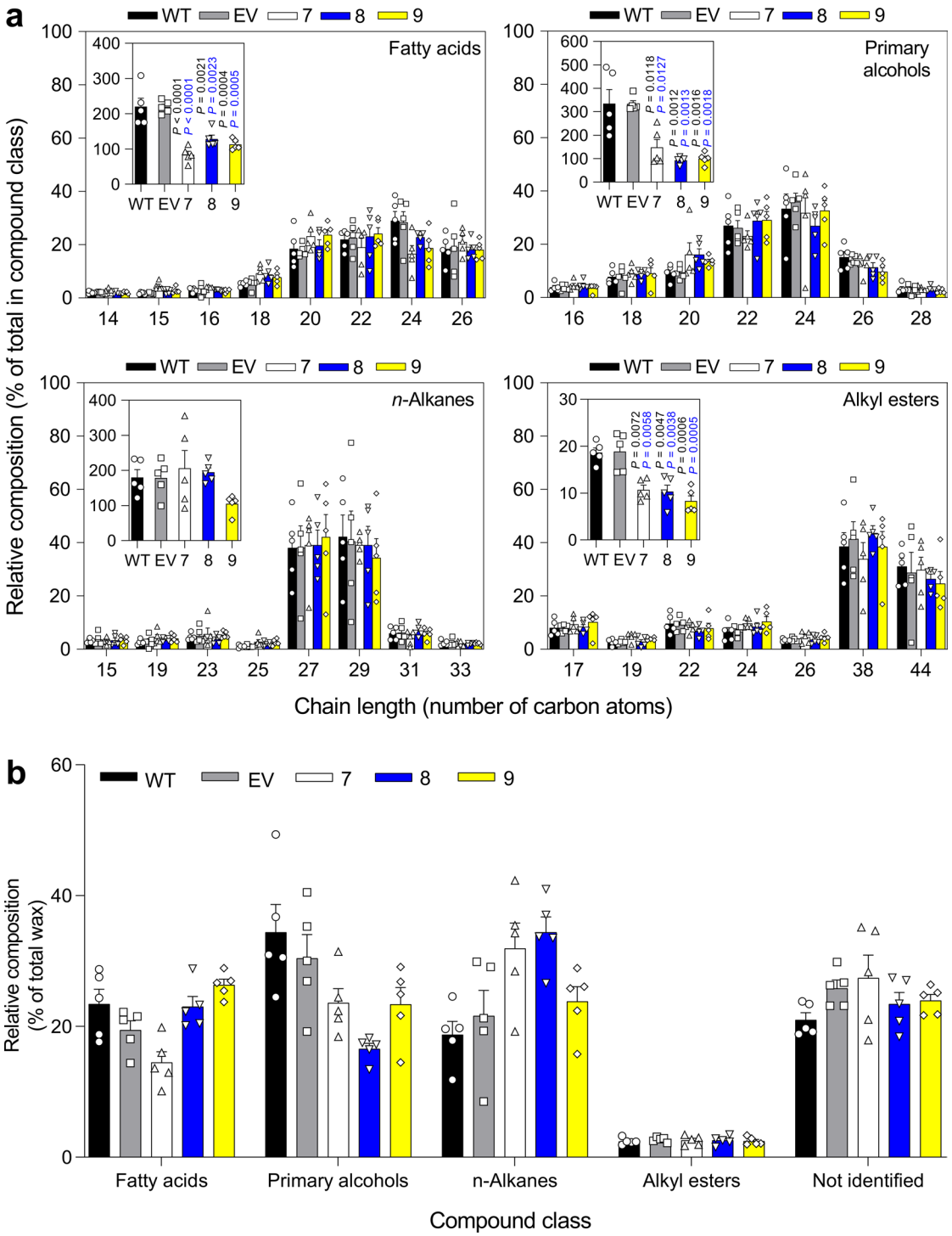

Extended Data Fig. 1 | Effect of *PhABCG12* downregulation on cuticle composition of 2-day-old petunia petals. a, Wax composition by major constituent classes: fatty acids, primary alcohols, *n*-alkanes, and alkyl esters in 2-day-old flowers of wild type (WT), EV control and transgenic lines 7, 8, and 9 collected at 10 PM. Relative amount of each wax constituent is presented as a percentage of the total in their respective compound class. X axis represents the chain length (number of carbon atoms) for each constituent. Inset graphs show total amount of each class (μg/g DW). Data are means ± s.e.m. (n = 5 biological replicates). *P* values were determined by two-way ANOVA with the Tukey's multiple comparisons test relative to the corresponding WT (black) and EV (blue) controls. **b**, Relative abundances of major constituent classes: fatty acids, primary alcohols, *n*-alkanes, and alkyl esters (shown in a) in wax of 2-day-old flowers of WT, EV control and transgenic lines 7, 8, and 9 collected at 10 PM. Data are means ± s.e.m. (n = 5 biological replicates).

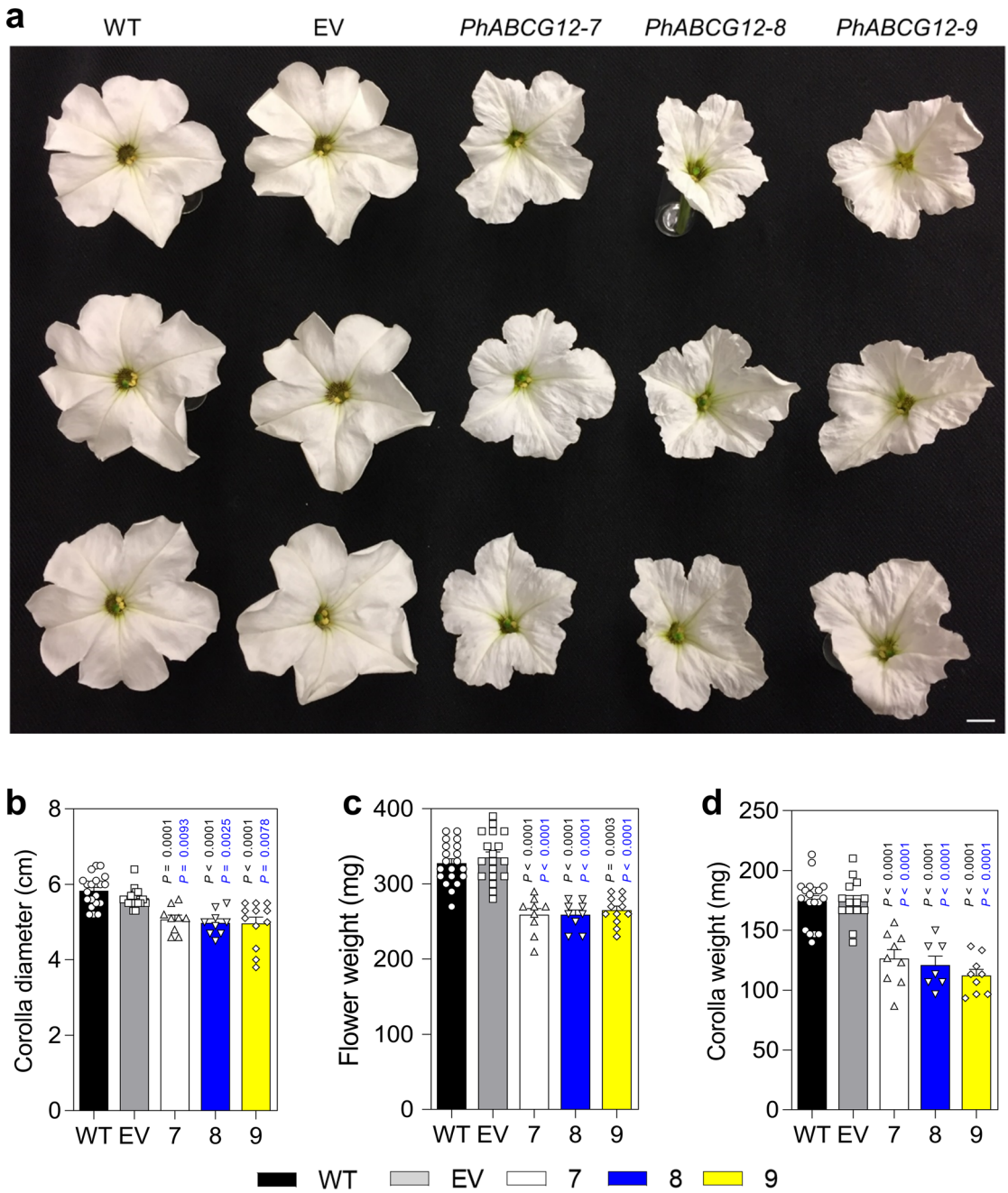

Extended Data Fig. 2 | Effect of *PhABCG12* downregulation on petunia flower phenotype. a, Representative 2-day-old flowers from wild type (WT), empty vector control (EV) and 3 independent *PhABCG12*-RNAi lines (7, 8 and 9). **b**, Corolla diameter, (**c**) flower weight and (**d**) corolla weight from WT, empty vector (EV)-transformed flowers and 3 independent *PhABCG12*-RNAi lines (7, 8 and 9). Data are means ± s.e.m. In **b** and **c**, n = 20 biological replicates for WT, n = 18 biological replicates for EV; and n = 9, 9 and 12 biological replicates for *PhABCG12* lines 7, 8, and 9, respectively; in **d**, n = 19 biological replicates for WT, n = 14 biological replicates for EV; and n = 9, 7 and 9 biological replicates for *PhABCG12* lines 7, 8, and 9, respectively. *P* values were determined by two-way ANOVA with the Tukey's multiple comparisons test relative to the WT (black) and EV (blue) controls. Scale bar in **a**, 1 cm.

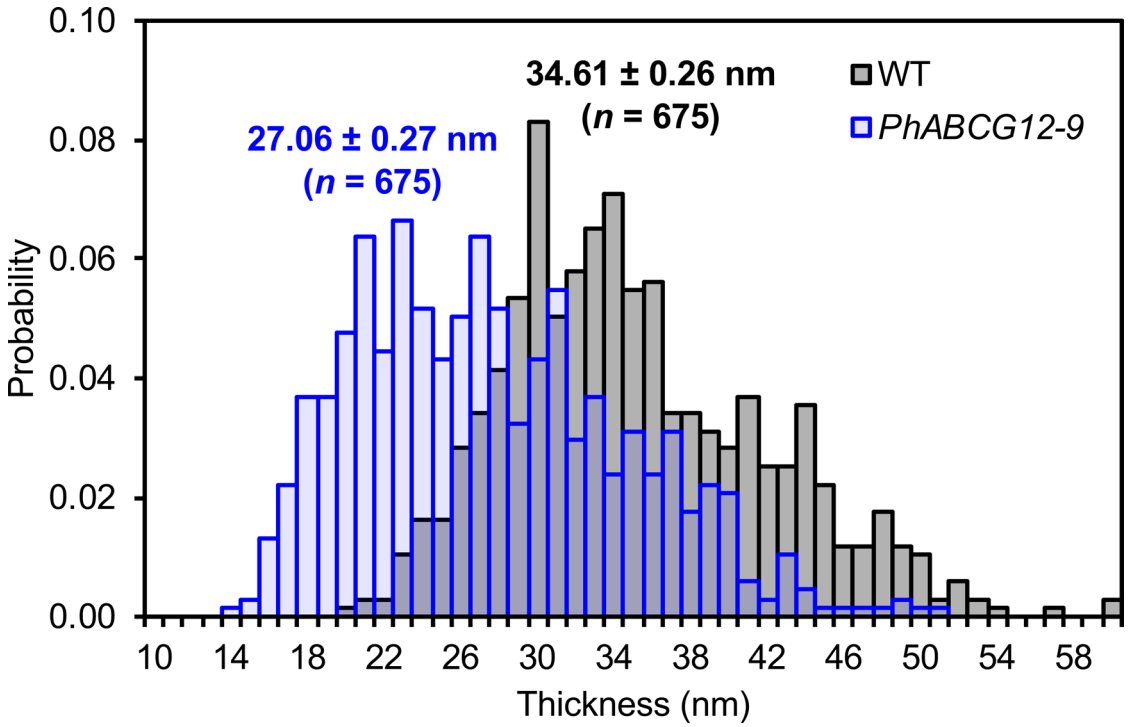

Extended Data Fig. 3 | Histogram showing cuticle thickness distribution in wild-type and *PhABCG12* petunia flowers. Cuticle thickness probability distribution in epidermal cells of 2-day-old wild type (WT) and *PhABCG12*-RNAi line 9 flowers. To be consistent cuticle thickness was measured only in conical cells. The distribution is presented as the probability of different cuticle thickness values over 675 measurements. Data are means ± s.e.m. (n = 675 measurements). Measurements were taken from discreet locations in a minimum of 11 cells per genotype.

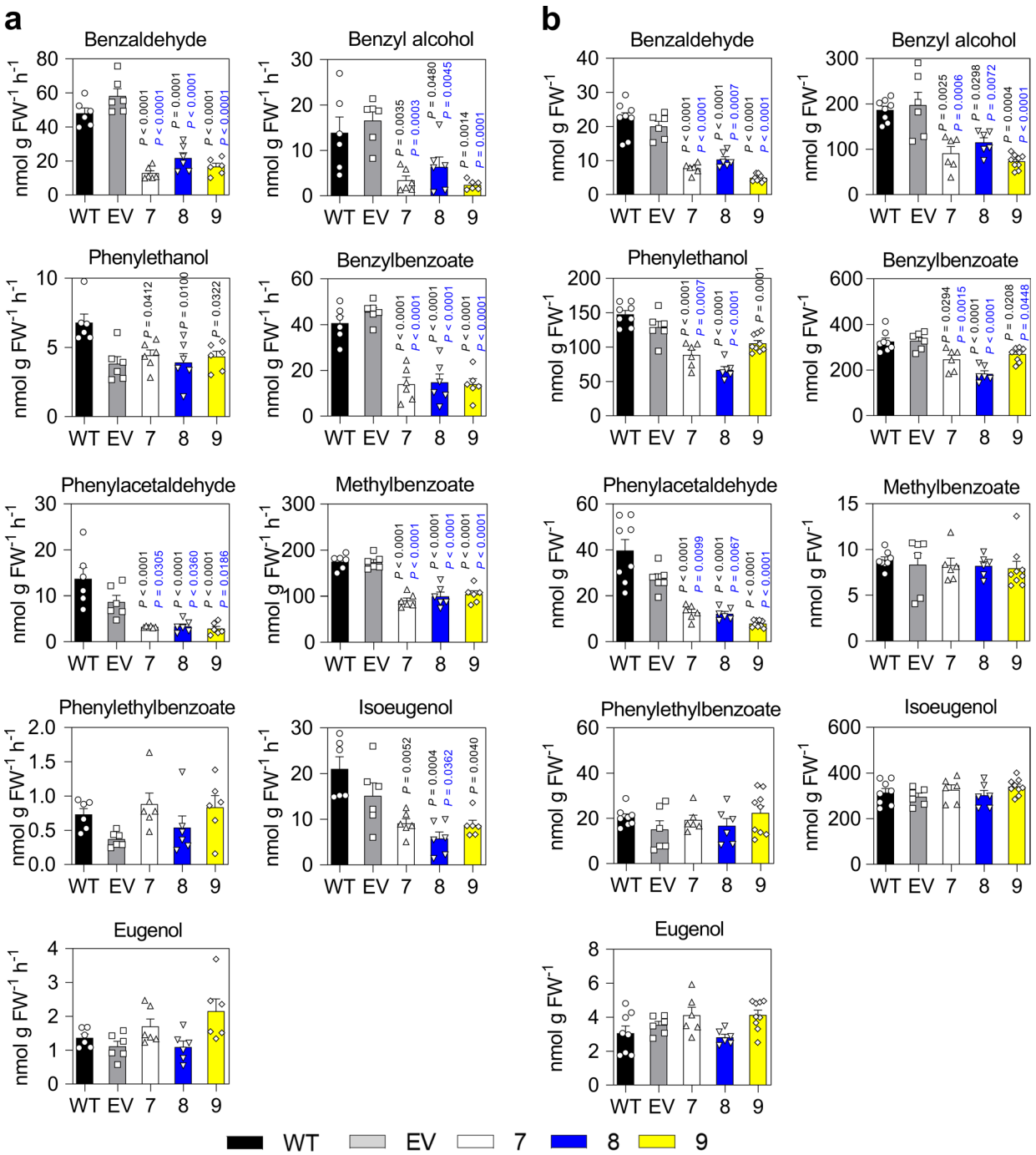

Extended Data Fig. 4 | Effect of *PhABCG12* downregulation on emissions and internal pools of individual benzenoid/phenylpropanoid volatiles in 2-day-old petunia flowers. Emission rates (**a**) and internal pools (**b**) of individual VOCs in wild type (WT), empty vector (EV) control and three independent *PhABCG12*-RNAi lines (7, 8 and 9). Data are means ± s.e.m. (in **a** n = 6 biological replicates for all samples; and in **b**, n = 8 biological replicates for WT, n = 6 biological replicates for EV, *PhABCG12*-RNAi lines 7 and 8; and n = 9 biological replicates for *PhABCG12*-RNAi line 9). *P* values were determined by two-way ANOVA with the Tukey's multiple comparisons test relative to the corresponding WT (black) and EV (blue) controls.

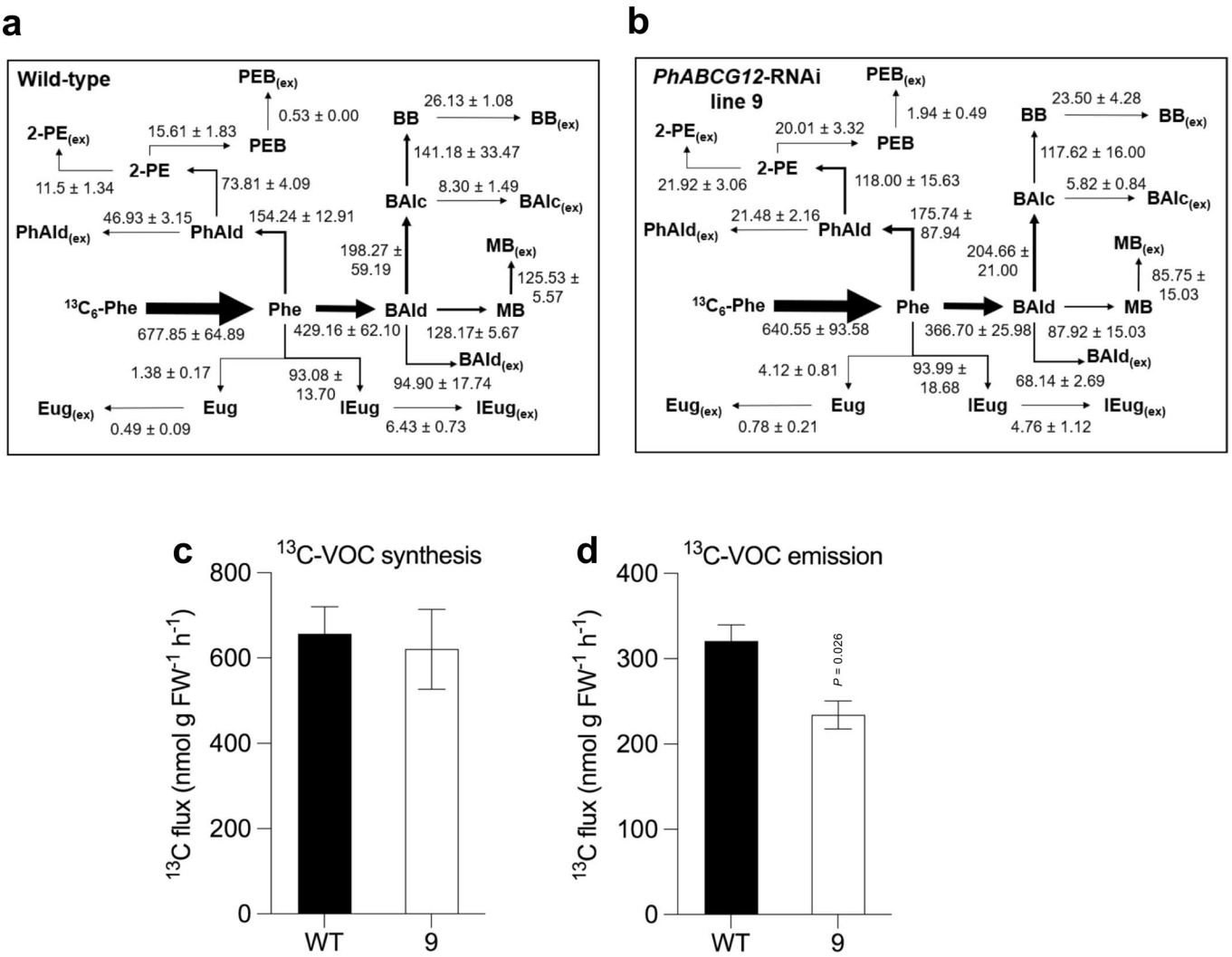

Extended Data Fig. 5 | Metabolic flux analysis of benzenoid and phenylpropanoid VOCs from petunia flowers supplied with 150 mM $^{13}C_6$-phenylalanine. Metabolic flux maps of 2-day-old wild-type **(a)** and *PhABCG12-9* **(b)** petunia petals fed with 150 mM $^{13}C_6$-Phe. Fluxes were obtained from time-course measurements of label incorporation in the endogenous pools and headspace collections of Phe-derived VOCs. Arrow thickness reflects the relative value of fluxes normalized to the incoming flux (turnover of $^{13}C_6$-Phe). BAlc, benzyl alcohol; BAld, benzaldehyde; BB, benzylbenzoate; Eug, eugenol; IEug, isoeugenol; MB, methylbenzoate; 2-PE, 2-phenylethanol; PEB, phenylethylbenzoate; and PhAld, phenylacetaldehyde. The total labeled biosynthetic **(c)** and emission **(d)** fluxes shown in **(a)** and **(b)**. Flux values are given in nmol·g FW^{-1}·h^{-1}. Data are the mean ± s.e.m. of total biosynthetic and emission fluxes calculated from the regression of time-dependent VOC pools and emission collections. Regression was performed using all data points simultaneously from biological replicates to obtain flux distribution values. Standard error of calculated fluxes were determined based on the propagation of measurement standard errors (n = 3 biological replicates) and the model regression error. *P* value was determined by unpaired two-tailed Student's *t*-test relative to wild type.

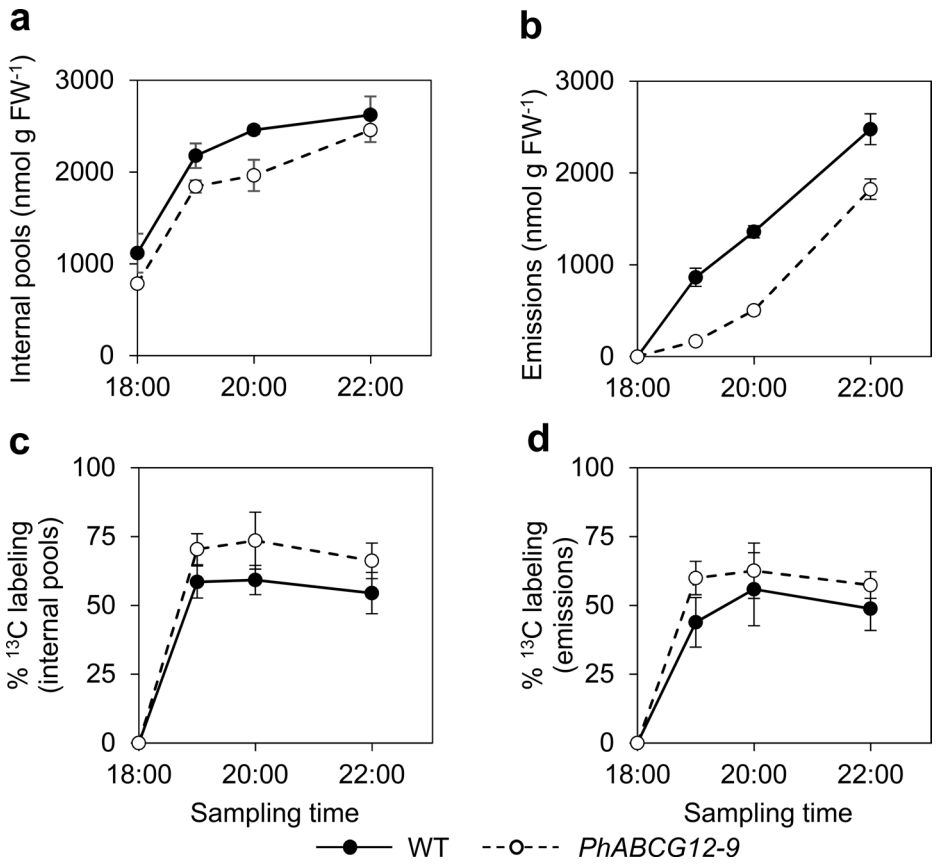

Extended Data Fig. 6 | Pool sizes and isotopic abundances of total endogenous (internal pools) and exogenous (emitted) VOCs in control and *PhABCG12-9* line petunia petals fed with 150 mM $^{13}C_6$-Phe. Total internal pools **(a)** and emissions **(b)** of VOCs from wild-type (WT) and *PhABCG12-9* petunia corollas supplied with 150 mM $^{13}C_6$-Phe for 4 h. Isotopic labeling of internal pools **(c)** and emitted volatiles **(d)** over 4 h, from 6 PM till 10 PM. Data are means ± s.e.m. (n = 3 biological replicates).

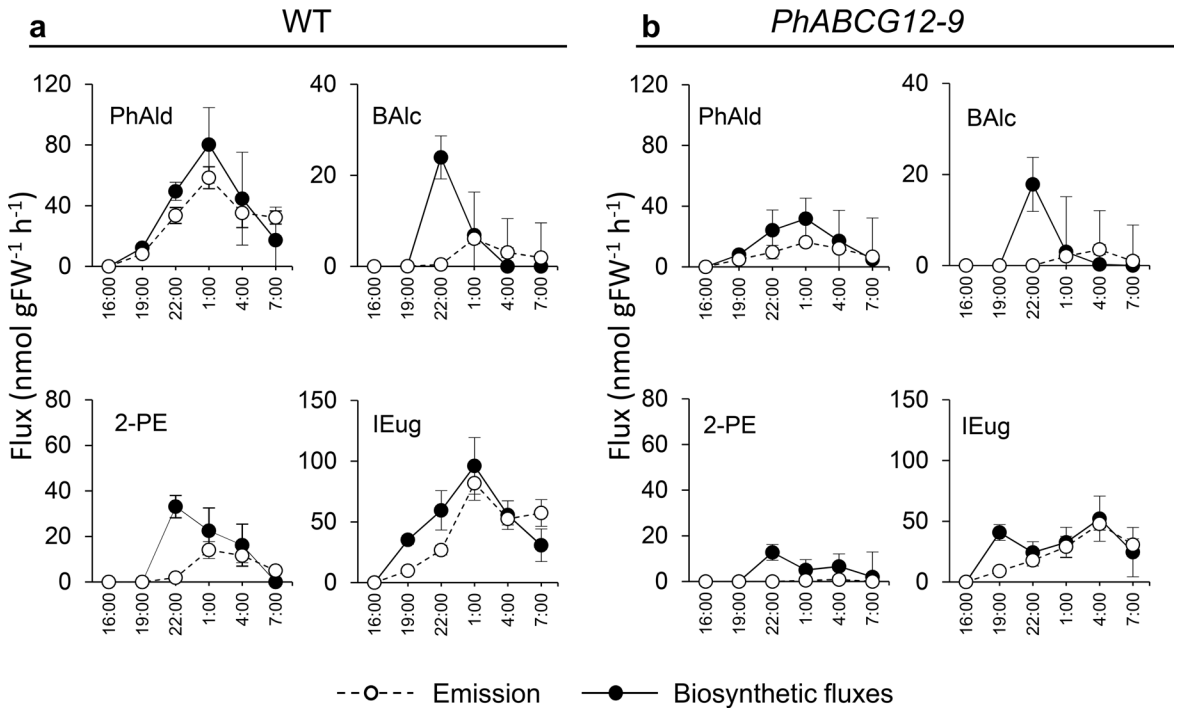

Extended Data Fig. 7 | Effect of *PhABCG12* downregulation on emission and biosynthetic fluxes of individual benzenoid/phenylpropanoid VOCs. Emission and biosynthetic fluxes for individual benzenoid/phenylpropanoid VOCs in 2-day-old wild-type (WT) **(a)** and *PhABCG12-9* **(b)** petunia flowers. BAlc, benzyl alcohol; IEug, isoeugenol; 2-PE, 2-phenylethanol; PhAld, phenylacetaldehyde. Data are means ± s.e.m. (n = 3 biological replicates).

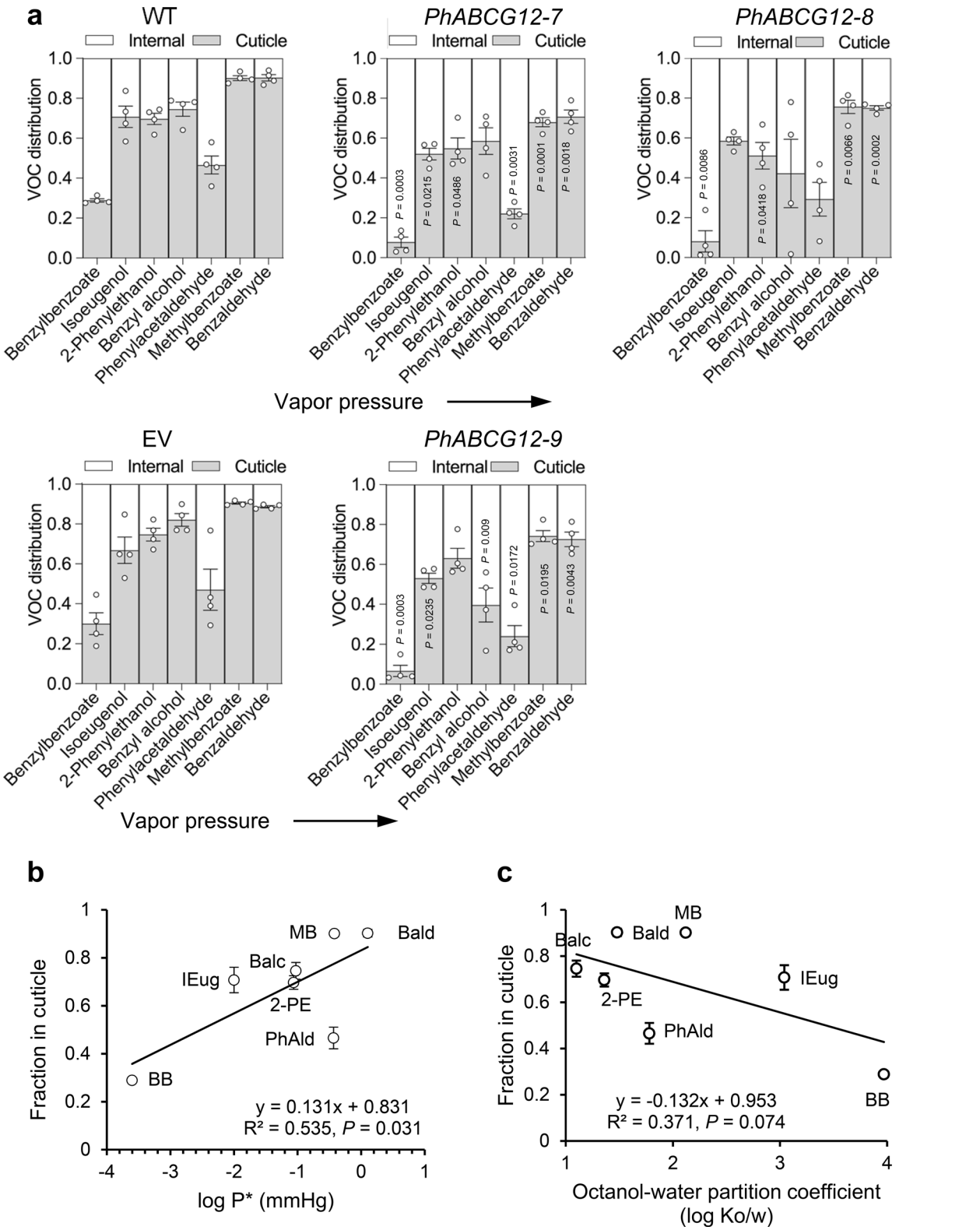

Extended Data Fig. 8 | Effect of *PhABCG12* downregulation on cellular distribution of individual benzenoid/phenylpropanoid VOCs in 2-day-old petunia flowers. a, Distribution of individual VOCs in wild-type (WT), empty vector control (EV) and *PhABCG12*-RNAi lines 7, 8 and 9. VOCs are shown in order of increasing volatility (left to right). Data are means ± s.e.m. (n = 4 biological replicates). *P* values were determined by unpaired two-tailed Student's *t*-test relative to corresponding wild type. **b**, **c**, Relationships between distribution of individual VOCs in the cuticle and their corresponding **(b)** vapor pressure and **(c)** octanol-water partitioning coefficient. Data are means ± s.e.m. (n = 4 biological replicates). In **b** and **c**, Pearson correlation coefficients (R^2) and corresponding *P* values are shown. BAlc, benzyl alcohol; BAld, benzaldehyde; BB, benzylbenzoate; IEug, isoeugenol; MB, methylbenzoate; 2-PE, 2-phenylethanol; PhAld, phenylacetaldehyde.

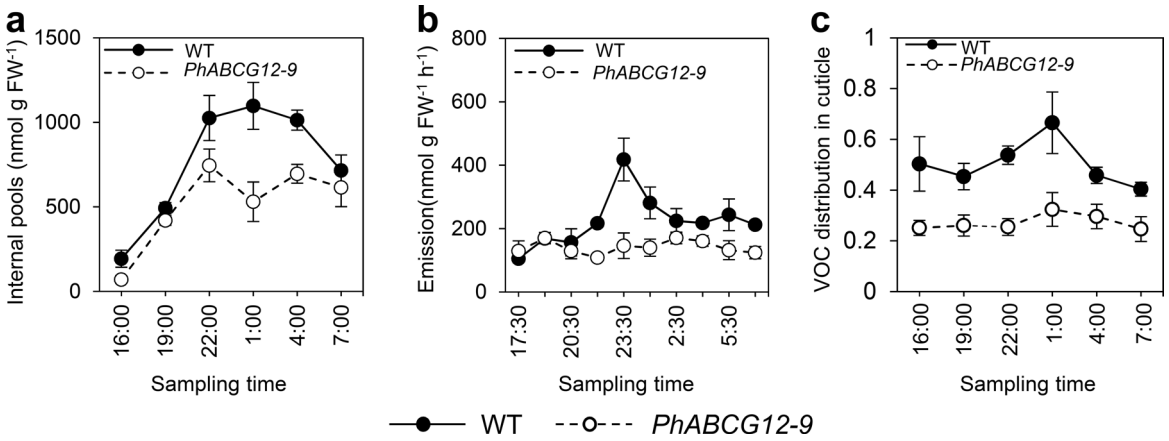

Extended Data Fig. 9 | Total internal pools, emissions and distribution in cuticle of benzenoid/phenylpropanoid VOCs in 2-day-old petunia flowers around peak of emission. Total internal pools **(a)**, emissions **(b)** and distribution in cuticle **(c)** of VOCs collected from wild-type (WT) and *PhABCG12-9* flowers over 15 h period. Data are means ± s.e.m. (n = 3 biological replicates in **a** and **b**; and n = 6 biological replicates in **c**). In **c**, *PhABCG12-9* VOC distribution in cuticle was statistically different ($P < 0.0001$) from WT based on two-way ANOVA.

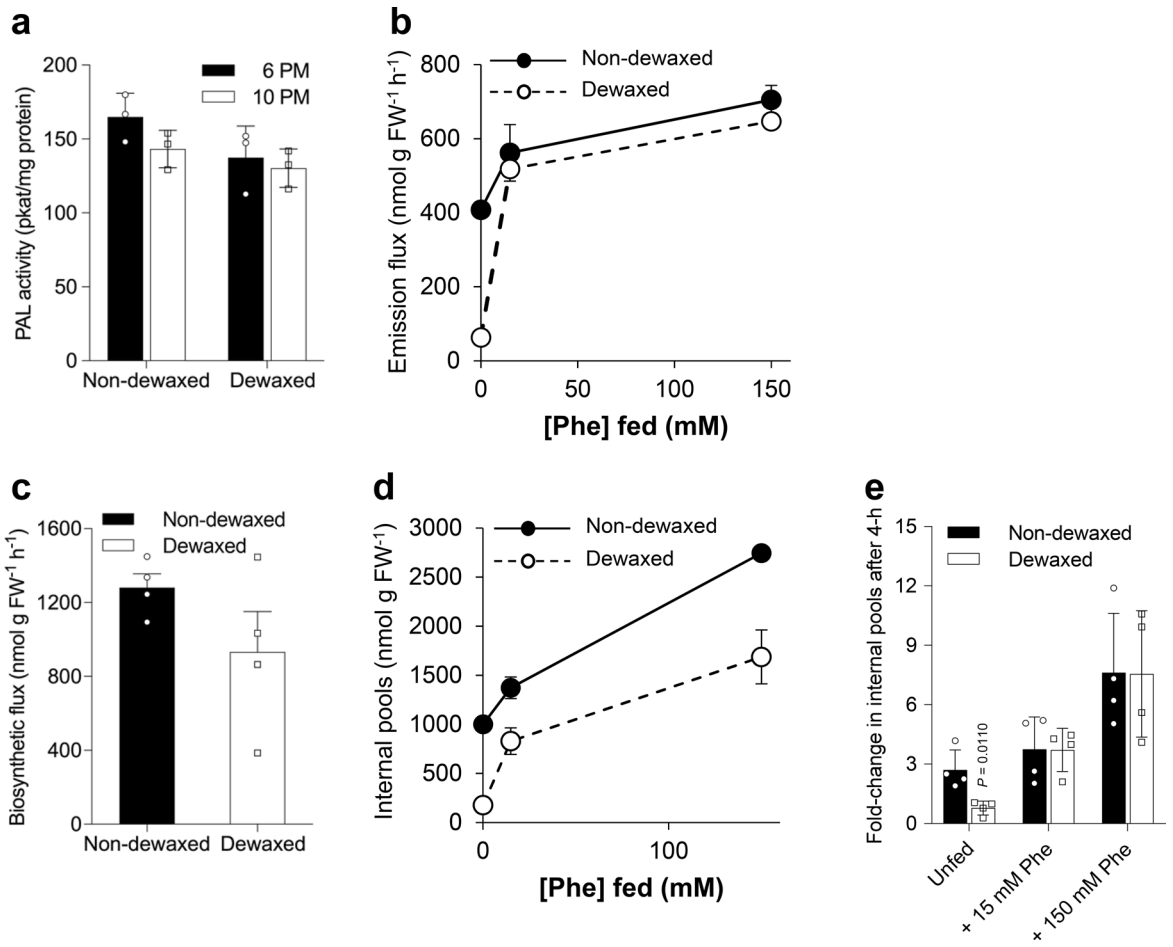

Extended Data Fig. 10 | Analysis of metabolic potential of petunia flowers after dewaxing. a, PAL activity detected in nondewaxed and dewaxed 2-day-old wild-type flowers in the beginning (6 PM) and the end (10 PM) of scent collection period. Data are means ± s.e.m. (n = 3 biological replicates). PAL activity was not statistically different between nondewaxed and dewaxed petals ($P = 0.1476$ and 0.2824 for 6 PM and 10 PM, respectively, determined by two-tailed Student's *t*-test). **b**, Volatile emission from nondewaxed and dewaxed wild-type flowers upon feeding different (0 - 150 mM) Phe concentrations. **c**, VOC biosynthetic fluxes in nondewaxed and dewaxed wild-type flowers fed with 150 mM Phe. **d**, Internal VOC pools in nondewaxed and dewaxed wild-type flowers upon feeding different (0 -150 mM) Phe concentrations. **e**, Fold-change in VOC internal pools from 6 PM to 10 PM in nondewaxed and dewaxed wild-type flowers upon feeding different (0 - 150 mM) Phe concentrations. *P* values were determined by unpaired two-tailed Student's *t*-test relative to corresponding non-dewaxed samples. Data in **b** - **e** are means ± s.e.m. (n = 4 biological replicates).

nature research

Corresponding author(s): Natalia Dudareva

Last updated by author(s): Aug 28, 2020

Reporting Summary

Nature Research wishes to improve the reproducibility of the work that we publish. This form provides structure for consistency and transparency in reporting. For further information on Nature Research policies, see our Editorial Policies and the Editorial Policy Checklist.

Statistics

For all statistical analyses, confirm that the following items are present in the figure legend, table legend, main text, or Methods section.

n/a	Confirmed	
☐	☒	The exact sample size (*n*) for each experimental group/condition, given as a discrete number and unit of measurement
☐	☒	A statement on whether measurements were taken from distinct samples or whether the same sample was measured repeatedly
☐	☒	The statistical test(s) used AND whether they are one- or two-sided *Only common tests should be described solely by name; describe more complex techniques in the Methods section.*
☒	☐	A description of all covariates tested
☒	☐	A description of any assumptions or corrections, such as tests of normality and adjustment for multiple comparisons
☐	☒	A full description of the statistical parameters including central tendency (e.g. means) or other basic estimates (e.g. regression coefficient) AND variation (e.g. standard deviation) or associated estimates of uncertainty (e.g. confidence intervals)
☐	☒	For null hypothesis testing, the test statistic (e.g. *F*, *t*, *r*) with confidence intervals, effect sizes, degrees of freedom and *P* value noted *Give P values as exact values whenever suitable.*
☒	☐	For Bayesian analysis, information on the choice of priors and Markov chain Monte Carlo settings
☒	☐	For hierarchical and complex designs, identification of the appropriate level for tests and full reporting of outcomes
☐	☒	Estimates of effect sizes (e.g. Cohen's *d*, Pearson's *r*), indicating how they were calculated

Our web collection on statistics for biologists contains articles on many of the points above.

Software and code

Policy information about availability of computer code

Data collection	GC-MS data were collected and analyzed using Agilent MassHunter Workstation Software v.B. 07.01. qRT-PCR data were collected using StepOne v.2 .2.2. LC-MS/MS data were collected and analyzed using Analyst 1.5.1 software. Confocal images were collected and analyzed using Zeiss Efficient Navigation (ZEN)-Black Edition software (Zen 2.3 SP1).
Data analysis	GC-MS data were analyzed using Agilent MassHunter Workstation Software v.B. 07.01, TEM images of petals were anayzed by ImageJ software version 1.52a, PAL activity by HPLC analysis was performed using Open LAB CDS Chemstation Rev. C.01.08[210]. LC-MS/MS data were analyzed using Analyst 1.5.1 software. RNAi constructs were analyzed using Sol Genomics Network VIGS Tool (http://vigs.solgenomics.net/).

For manuscripts utilizing custom algorithms or software that are central to the research but not yet described in published literature, software must be made available to editors and reviewers. We strongly encourage code deposition in a community repository (e.g. GitHub). See the Nature Research guidelines for submitting code & software for further information.

Data

Policy information about availability of data

All manuscripts must include a data availability statement. This statement should provide the following information, where applicable:

- Accession codes, unique identifiers, or web links for publicly available datasets
- A list of figures that have associated raw data
- A description of any restrictions on data availability

The authors declare that all the data supporting the fundings of this study are available within the paper and its supplementary information files or from the corresponding author upon reasonable request. Source data are provided with this paper. Petunia axillaris genomic data were obtained from http://solgenomics.net using Petunia axillaris v1.6.2 genome database.

Field-specific reporting

Please select the one below that is the best fit for your research. If you are not sure, read the appropriate sections before making your selection.

☒ Life sciences ☐ Behavioural & social sciences ☐ Ecological, evolutionary & environmental sciences

For a reference copy of the document with all sections, see nature.com/documents/nr-reporting-summary-flat.pdf

Life sciences study design

All studies must disclose on these points even when the disclosure is negative.

Sample size	Precise sample sizes were chosen based on previously published work in the field (Lynch et al. 2020; Adebesin et al., 2017). Shown results were evaluated by statistical analysis as indicated in corresponding figure legends.
Data exclusions	No data exclusion
Replication	At least three biological replicates were performed for each experiments and all attempts at replication were successful.
Randomization	Plants were randomized in greenhouse, and sample orders were randomized during analysis.
Blinding	Blinding is not necessary because results are quantitative for all experiments, and not subjective. Blinding was not possible in these experiments, as samples were analyzed immediately after collection, and the treatments were known to the investigator.

Reporting for specific materials, systems and methods

We require information from authors about some types of materials, experimental systems and methods used in many studies. Here, indicate whether each material, system or method listed is relevant to your study. If you are not sure if a list item applies to your research, read the appropriate section before selecting a response.

Materials & experimental systems

n/a	Involved in the study
☒	☐ Antibodies
☒	☐ Eukaryotic cell lines
☒	☐ Palaeontology and archaeology
☒	☐ Animals and other organisms
☒	☐ Human research participants
☒	☐ Clinical data
☒	☐ Dual use research of concern

Methods

n/a	Involved in the study
☒	☐ ChIP-seq
☒	☐ Flow cytometry
☒	☐ MRI-based neuroimaging